Alma Mater Studiorum - Università di Bologna

SCUOLA DI SCIENZE

Dipartimento di Chimica Industriale "Toso Montanari"

Corso di Laurea Magistrale in

Chimica Industriale

Classe LM-71 - Scienze e Tecnologie della Chimica Industriale

Synthesis and characterization of heteroleptic Cu(I) complexes based on quinolin-yl-1,2,3-triazole and pyridin-yl-1,2,3 triazole

Tesi di laurea sperimentale

CANDIDATO

Tobia Barchi

RELATORE

Prof. ssa Letizia Sambri

CORRELATORE

Dr. ssa Claudia Bizzarri

Anno Accademico 2019-2020

To the memory of Clara Immerwahr

Acknowledgment

I would like to thank Dr. Claudia Bizzarri, who has patiently followed me in these months and Prof. Bräse, who hosted me in his research group. I have to thank all people that have supported me in the last five years.

INDEX

1 INTRODUCTION

1.1 Energy and quality of life

Quality of life is a general term for the quality of various domains in life. It is a standard level that consists in the expectations of an individual or society for a good life. These expectations are guided by the values, goals and socio-cultural context in which an individual lives. It is a subjective and multidimensional concept that defines a standard level for emotional, physical, material and social well-being.

This concept is hard to evaluate by a single indicator, anyway it is possible to try to describe quality of life by a small number of variables. Infant mortality (IM, deaths per 1000 live births) and female life expectancy (LE) are possibly the two best (unambiguous) indicators of the physical quality of life. Infant mortality is a summary measure, which reflects excellently the complex effects of nutrition, health care, and environmental exposures on the most vulnerable group in any population. The female life expectancy includes long-term effects of these critical variables. At the beginning of the 21th century the lowest IM rates were in the richest country (Japan, Western Europe, North America and Oceania) and, on the other side, the highest IM rates (>100) were in the poorest countries in the world (mainly in Africa). Acceptable IM rates (<30) corresponded to annual per capita energy use of at least 30-40 GJ/year, but very low IM rates (<20) could be only found in countries using at least 60 GJ/year per capita and the lowest rates (<10) were not found in any countries using less than 110 GJ/year per capita. Increased energy use beyond this level is not associated with any further declines of IM. Female life expectancy is in accordance with the first variable: the lowest female LE (<45 years) is in African poorest countries, the highest (>80 years) in Japan, Canada and several EU nations. Again, high female LE (>70 years) requires at least 45-50 GJ/year per capita and very high female LE (>80 years) requires at least 110 GJ/year per capita.

A third important variable, the Human Development Index (HDI), was studied by Smil (2008). The HDI is more complex than the variables mentioned above: it is calculated from life expectancy at birth, adult literacy, combined with education enrolment. Also in this case, we can observe a correlation between HDI and annual per capita energy: high HDI (>0,8) can be reached with 65 GJ/year and there are no additional gains above 110 GJ/year. In conclusion, the quality of life grows up by non-linear trend with increasing available energy until 110 GJ/year per capita. (Figure 1.1) [1,2]

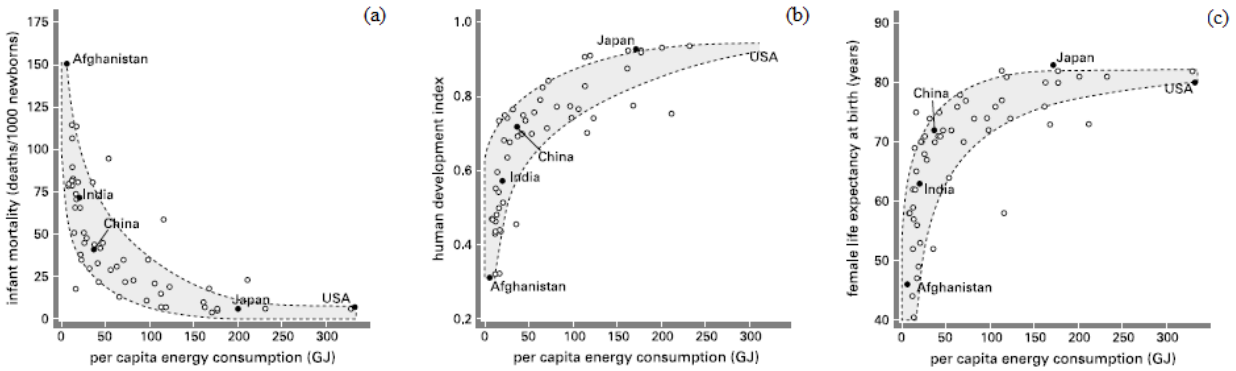

Figure 1.1 *Comparison among average per capita energy use and (a) infant mortality, (b) Human Development Index, (c) female life expectancy at birth.* [1]

Furthermore, it is easily seen a huge per capita energy consumption gap between the richest and the poorest countries, after looking at Figure 1.1. Improving the access to energy for poorest countries, increasing the quality of life and, in the end, reducing this gap should be a world goal. This target is not simply based on philanthropic principles, but it replies to political and economic requests: in the whole globe, people escape from misery and seek better living conditions and these increasing flows generate tensions.

The ideal parameters for 2050 would be the following: with an estimated global population of 9 billions, the per capita consumption would be 2.8 toe/year (=117 GJ/year), the demands for primary energy consumption should be 25.2 Gtoe*[1]/year. Such amount of energy is twice as much as the present level; this target is not impossible, if one considers that it is in line with the trend from 1980 to 2015, when the global energy demand was doubled.

Where can we find this energy?

This question is hard to answer. Fossil fuels are not a sustainable resource anymore, since their combustion releases CO_2 and increases the greenhouse effect.[3] For this reason the possible solutions to this problem must be directed towards the reduction of energy-use by rich countries and improving the transformation efficiency of primary energy. The overall composition of the energy-use and the proportions of the different energy sources must be changed; solar energy will play a key role in this process of transformation.[4]

*[1] *tonne of oil equivalent* (toe) is a unit of energy defined as the amount of energy released by burning one tonne of crude oil. 1 toe = 41.868 GJ

1.2 A Different use of Solar Energy

Where vegetation is rich, photochemistry may be left to the plants and by rational cultivation,[…]solar radiation may be used for industrial purposes. In the desert regions, unadapt to any kind of cultivation, photochemistry will artificially put their solar energy to practical uses. On the arid lands there will spring up industrial colonies without smokes and without smokestack; forest of glass tubes will extend over the plains and glass buildings will rise everywhere; inside of these will take place the photochemical processes that hitherto have been guarded secret of the plants, but that will have been mastered by human Industry.[5]

The use of sun light as energy source has several advantages: it is abundant, inexhaustible and well-distributed. However, it also has some disadvantages: the irradiation is not constant during the day and the year. Moreover, electrical power produced in this way needs to be stored, so additional materials must be exploited.[4,6] In the next paragraphs the problems will be discussed in details, especially focusing on the different typologies of use of solar energy and the advantages and disadvantages related to them.

1.2.1 Photovoltaic panels and electricity production

In a semiconductor such as silicon, the molecular orbitals interact to form energy bands. The electronic structure of semiconductors is constituted by two bands: the lowest energy band is full of electrons and it is called conduction band (VB), the highest energy band is empty and it is called conduction band (CB), the energy gap between these two bands is called band-gap energy (Eg). If a photon with $h\upsilon$=Eg is absorbed by semiconductor, electron will jump from VB to CB; as a consequence of this, an electron vacancy is formed (h^+, hole) on VB.

Small quantity of some elements are added to silicon to increase the conductivity of semiconductors, varying the energy of their VB or CB; this technique is called *doping*. N-type doping consists in impurity of five valence electrons (like As, P), the conductivity increases because the CB is partly filled with electrons. On the other hand, P-type doping consists in impurity of three valence electrons (like Ga, In), the conductivity increases because the VB is partly filled with holes. Photovoltaic cells are made up by n-doped and p-doped silicon joined together by p-n junction. A hole-electron pair is produced by photon absorption and, then, it is transported through an electrical circuit where it can be used as electric energy. The p-n junction plays a key-role because it cannot

afford a charge recombination.[7] The use of photovoltaic panels has several advantages: easy scale-up, no moving parts, very low maintenance costs, installation possible on existing platforms with no land consumption, decentralization of the electricity production system, production in off-grid isolated areas. The efficiency of energy conversion from light to electricity is 15-22% and it is comparable or higher than successful devices (like cars or light bulbs). In 2014 PV technology produce, only less than 1% of world energetic demand. [8]

The main materials are abundant and not toxic (e.g copper, silver, aluminium, silicon and plastics), but a crucial issue is represented by the world stores of elements used to doping semiconductor (these elements often have a concentration close to ppm). In fact In, Ga, Se, Te and Cd reserves are less abundant than previous element and it will be not possible satisfy the world requests in a possible world energy transition.[4][9]

In the last decades two new different photovoltaic technologies have been studied: dye-sensitized solar cells (DSSC) or "Graetzel Cells" (from the name of the inventor)[10] and organic photovoltaics (OPV). These technologies can be easily installed in "non-conventional" building positions (e.g. windows and facades) and, more important, their production requires lower quantity and quality of raw materials than traditional photovoltaic panels. The DSSC consist in a semiconductor covered with a chromophoric organic dye. Although the semiconductor cannot absorb visible light, it has a good stability (as TiO_2). The organic dye absorbs visible light and transfers the excited electron to the inorganic semiconductor. The electron flows to anode and the electronic lack is filled by an electron from a redox mediator (I_2/I_3^-); finally, the redox mediator is reduced back at the cathode (figure 1.2). [4][7]

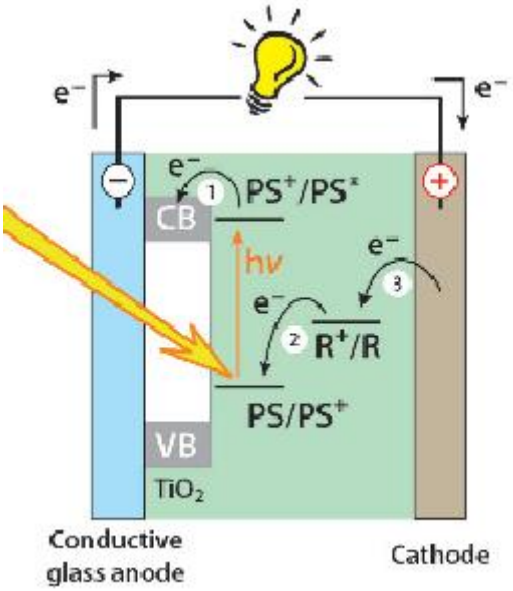

Figure 1.2 *Schematic operating principles of DCCS.* [4]

OPV are constituted by photoactive π-conjugated polymers and small organic molecules. The donor material (polymers) absorbs a photon, thus, an electron is promoted to the lower unoccupied molecular orbital (LUMO) of this material. The potential energy allows the diffusion of the excitation to donor/acceptor interface. At the interface, the excited electron of the donor material is transferred to the LUMO of the acceptor material, while a hole remains on the highest occupied molecular orbital (HOMO) of the donor. When the charge transfer (CT) takes place, the hole is collected at the anode and the electron is collected in the cathode (Figure 1.3). [4][11]

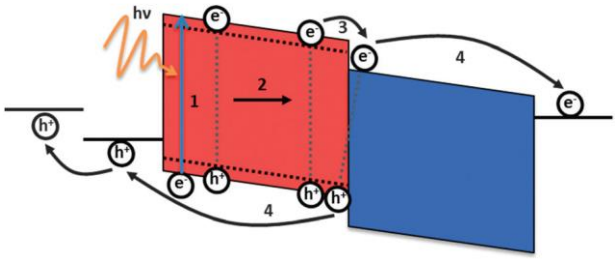

Figure 1.3 *Schematic operating principles of OPV.* [11]

Unfortunately, these technologies are still "young": the efficiency of energy conversion from light to electricity and lifetime are lower and the payback time is higher than traditional PV. No significant amount of electricity is produced from these new technologies, but in the last two decades these applications has been considerably improved. Anyway, the energetic efficiency and resistance to deterioration should be improved and the cost should be reduced: hopefully these targets will be reached in the next years. [4], [12]

1.2.2 Photosynthesis

Nature uses solar energy through a process called photosynthesis. Some plants and microorganisms produce carbohydrate and O_2 from water and CO_2, photoautotroph organisms require sun-light as energy source because the reaction is endergonic. (Figure 1.4).

$$CO_2 + H_2O \xrightarrow{sun\text{-}light} \text{Carbohydrate} + O_2$$

Figure 1.4 *Simplified scheme of the reagent and products of a photosynthetic reaction*

Photosynthesis can be divided in two different set of reactions. The first ones are called *Light reactions*, where the light energy is converted in "chemical energy" and O_2 is generated. The second ones are called *Dark reactions*, where the "chemical energy" supplies the necessary energy in the conversion CO_2 into carbohydrate. The organisms that are able to do photosynthetic reactions are

bacteria and plants and their processes have many similarities. However, in the next section only plants photosynthesis will be discussed.

Light reactions are summarized in three steps:

- *Light harvesting:* several hundreds of pigments act together as the photosynthetic unit, which is formed from light-harvesting antennae and the reaction centre. Chlorophyll is the main pigment used in green plants; these molecules are composed of a rigid, planar, conjugated porphyrin ring which can absorb solar light. A hydrophobic phytol chain, which can anchor the chlorophylls to photosynthetic membrane and Mg^{2+} ion, is coordinated with porphyrin ring (Figure 1.5). There are two different kinds of chlorophyll, **a** and **b**. Their chemical structures are quite similar but they absorb sunlight in two different regions of the spectrum. In order to use the whole sunlight spectrum, plants employ additional pigments, like carotenoids. The light-harvesting antennae absorb photons and the energy is quickly transferred through adjacent pigments (with a Coulombic long-range mechanism) to the reaction centre. This step occurs in few femtoseconds.

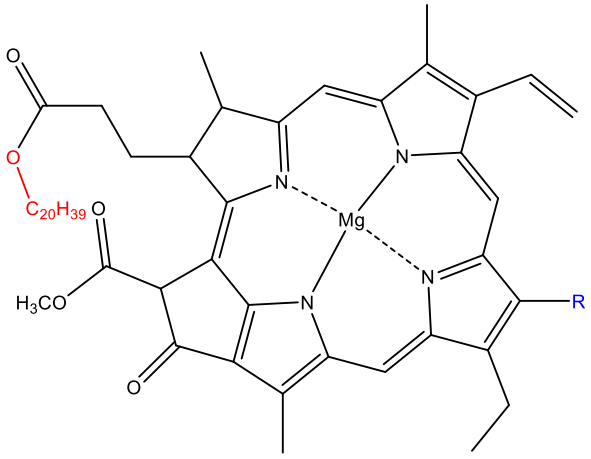

Figure 1.5 Structures of chlorophyll: R=CH_3 in **chlorophyll a** and R=CHO in **chlorophyll b**. The phytol chain is represented in red.

- *Charge separation and transport:* there are two different photosystems: PSII (reaction centre is P680) and PSI (reaction centre is P700). After light-harvesting process, the reaction centre P680 is in its excited state (P680*) acting as a very good electron-donor, so it reduces the electron acceptor 1 (EA_1). The reaction centre is oxidised ($P680^+$) and the EA_1 is reduced (EA_1^-). The process is similar for PSI: after light-absorption, the reaction centre P700 is in its excited state (P700*), it can reduce the electron acceptor 2 (EA_2). The reaction centre is oxidised ($P700^+$) and the EA_2 is reduced (EA_2^-) (Figure 1.6).

- *Water oxidation and energy storage:* The electron lack in P680 is filled back by H_2O electrons (sacrificial electron donor: SED): water is oxidised and oxygen is produced as co-product. This reaction is catalysed by Mn-complex catalyst. EA_1^- rapidly leaves its electron to the first electron transport chain, this electron reduces $P700^+$ in P700. EA_2^- is also oxidised by a second electron transport chain, but, in the end, nicotinamide adenine dinuclotide phosphate ($NADP^+$) is reduced in the reduced species (NADPH) (Figure 1.6). The electron flow between the electron transport chains produces an electrochemical gradient, it is used by enzyme (ATP-synthase) to produce adenosine triphosphate (ATP). ATP and NADPH are high energy molecules, plants produce these molecules from light-sun and, later, they use it to realize other endergonic reactions (as CO_2 fixation). [7], [13]

  In the dark reactions, plants produce carbohydrate from CO_2, the energy input is furnished from high-value energy compounds (NADPH and ATP), these molecules are produced on previous step. In this moment, six CO_2 pathways are known, but the two most famous are the Calvin-Benson-Bassham CBB cycle and the reductive acetic citric cycle. [3]

Intermediates and products of dark reactions, through anabolism processes, can became starch, cellulose, oil, and so on. Every year, photosynthesis produces more than 100 billion tons of dry biomass with energy conversion efficiencies between 0,1 and 1,0% (depends on origin). These substances can be used as biomass and the mankind can obtain energy (and fuel) from biomass. [14]

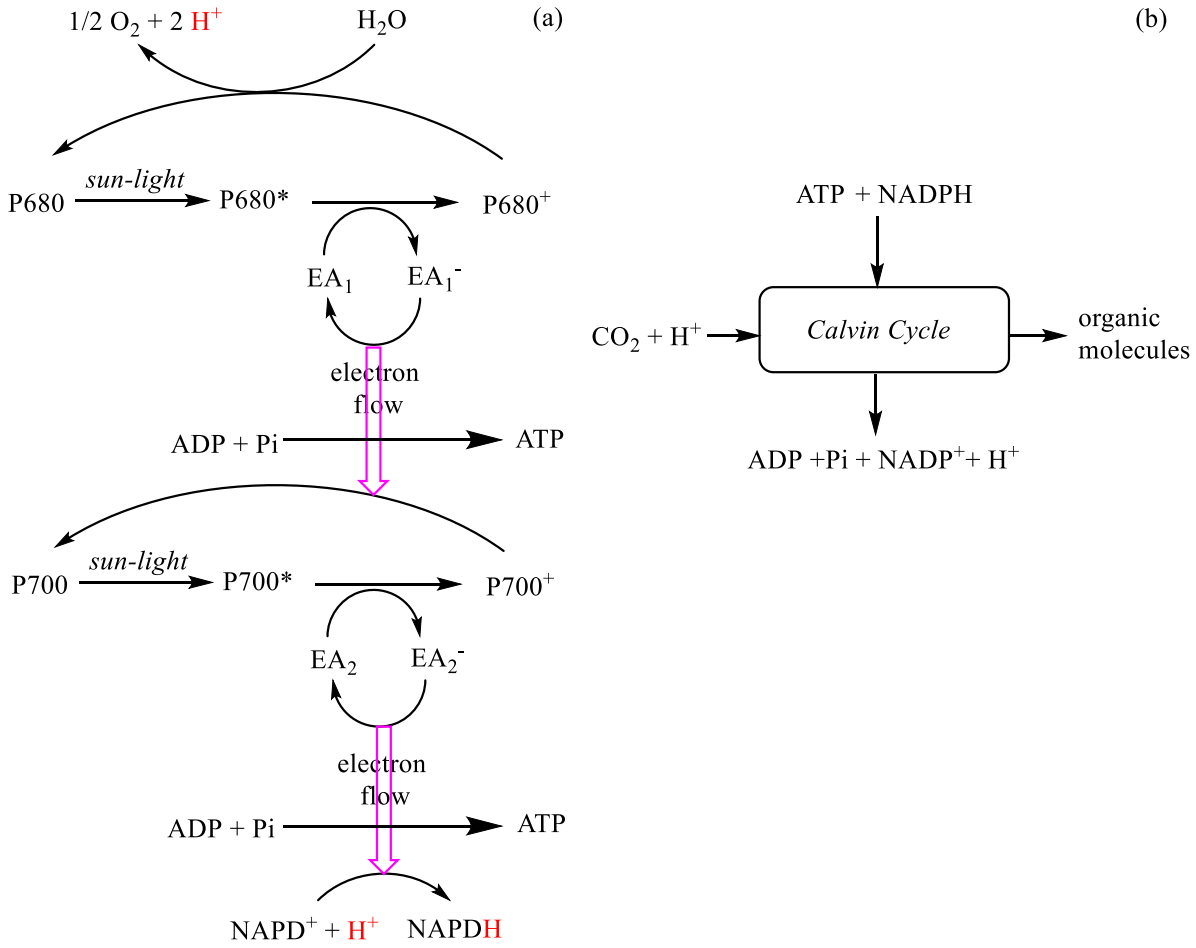

***Figure 1.6**: (a) Light reaction scheme NADPH and ATP are produced from water oxidation using sun-light (b) simplified scheme of Calvin cycle*

1.2.3 Artificial photosynthesis

Since the beginning of 1970s a new pathway has been explored [3]: the *artificial photosynthesis*. The end of this way is a process, which can efficiently use and store the sun-light to produce fuels, solvents and chemicals. An additional advantage of this concept is "close to zero CO_2 emission", in fact the starting material is atmospheric CO_2, so the artificial photosynthesis could highly reduce the anthropic CO_2 emission. Water is oxidised in O_2 and the electrons are used to reduce CO_2 in higher energy compounds as CH_4, CH_3OH, CO, formaldehyde, formate, oxalate or to reduce protons in H_2. (Figure 1.7)

$$CO_2 + 2\ e^- + 2\ H^+ \longrightarrow HCOOH$$

$$CO_2 + 2\ e^- + 2\ H^+ \longrightarrow CO + H_2O$$

$$2\ CO_2 + 2\ e^- + 2\ H^+ \longrightarrow (CO_2H)_2$$

$$CO_2 + 4\ e^- + 4\ H^+ \longrightarrow CH_2O + H_2O$$

$$CO_2 + 6\ e^- + 6\ H^+ \longrightarrow CH_3OH + H_2O$$

$$CO_2 + 8\ e^- + 8\ H^+ \longrightarrow CH_4 + 2\ H_2O$$

Figure 1.7: *Summary scheme of CO_2 reduction reactions*

With the purpose of make easier the study, the development and the improvement of this process, artificial photosynthesis is divided in two half-reactions: H_2O oxidising reaction and CO_2 reducing reaction. To supply the absence of the other half reaction, in the oxidising reaction a sacrificial electron acceptor (SEA) is used and, on the other side, in the reducing reaction a sacrificial electron donor (SED) is used. In this thesis, only the CO_2 reducing reaction is going to be discussed. The mechanism is summarised in Figure 1.8. A photosensitizer (PS) absorbs a photon, it goes in the excited state (PS*) and it is quenched by SED to generate reduced photosensitizer (PS^-) and oxidized SED (SED^+). Now PS^- can act as an excellent electron donor and it can reduce the catalyst (cat) in the reduced catalyst species (cat^-). So the cat^- can active and reduce the CO_2. (Figure 1.8). [15]

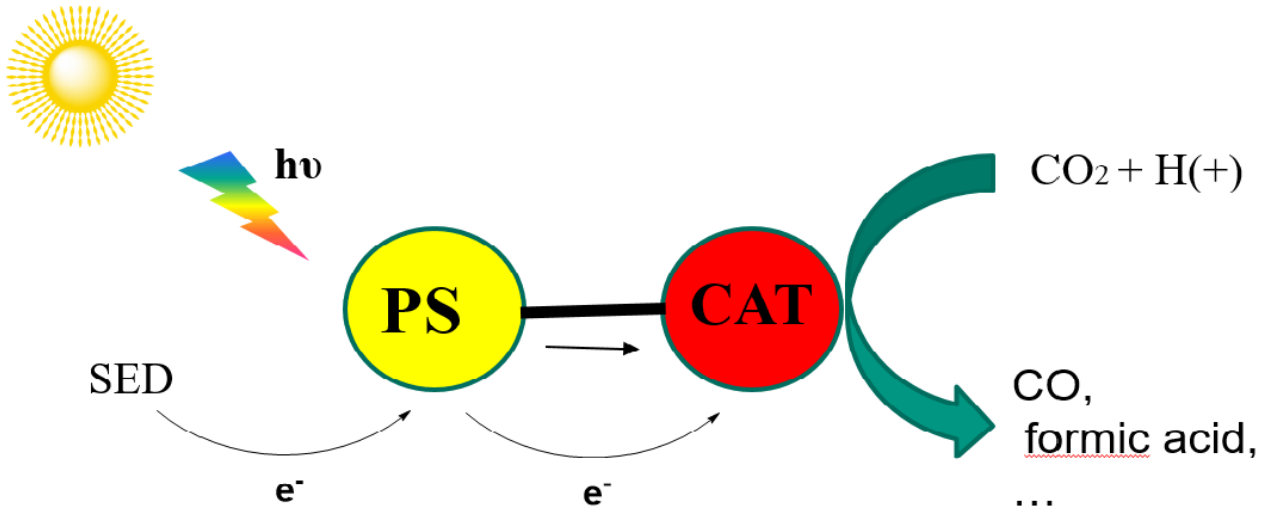

Figure 1.8 *Generic mechanism of artificial photosynthesis. PS absorb a photon, then it is reduced from SED and it cat reduce the cat, cat^- can reduce CO_2 in more energetic compounds. PS and cat can or cannot link together, sometimes a single molecule can work as PS and cat*

It is a hard task, because the CO_2 reduction is thermodynamically and kinetic disfavoured, so several catalysts has been tested and studied. The catalysts can be divided in two categories: homogenous and heterogeneous. [3], [15]

1.2.3.1 Heterogeneous catalysts: photoelectrochemical reduction and electrochemical reduction

The first step of this process is the CO_2 activation, where it can be reduced in two different radicals species:$\cdot CO_2^-$ **(1)** or, if a protons source is available, in CO_2H **(2)**. In this step the CO_2 changes its structure from linear to bent and it is the most energetic expensive step. In Figure 1.9, the possible mechanisms in different solvents are illustrated. In aprotic solvents the reaction involves in two different pathways: *(1)* CO_2 is reduced and adsorbed to electrode surface to produce intermediate **1**, then it reacts with CO_2 to produce intermediate **3**, finally it is reduced, CO and CO_3^{2-} are produced through disproportionation; *(2)* oxalate is produced through self-coupling of **1**. In protic solvents the reaction involves, also, in two different pathways: *(3)* intermediate **1** is produced like previous step, then it is reduced and reacts with 2 H^+, after electronic-arrangement CO and H_2O are produced; *(4)* in aqueous solvents the intermediate **2a** strips a proton from solvent and produce the intermediate **2b**, then it is reduced and produce formate, which is protonated and produce formic acid. [16][17]. Another important difference among solvents is the solubility of CO_2, for example in aqueous solutions CO_2 has 7-8 times lower solubility than methanol. In addition, CO_2 in aqueous solution is hydrated, CO_3^{2-} and HCO_3^- are generated and the study of CO_2 solubility became more complicated.[15]

Solvent is not the only variable that influence products distribution, also the electrode plays a crucial role. The electrodes are divided in two categories: CO producer metals (like Cu, Au, Ag, Zn, Pd, Ga) and $HCOO^-$ producer metals (Pb, Hg, In, Sn, Cd, Tl). Some types of electrodes (like Ni, Fe, Pt and Ti) cannot reduce CO_2 (or can reduce with very low selectivity) but in aqueous media can produce efficiently H_2, which is a very common by-product using previous electrodes [17]. H_2 can be used to storage energy from sun [4] or to reduce CO_2 in a different step. [18].

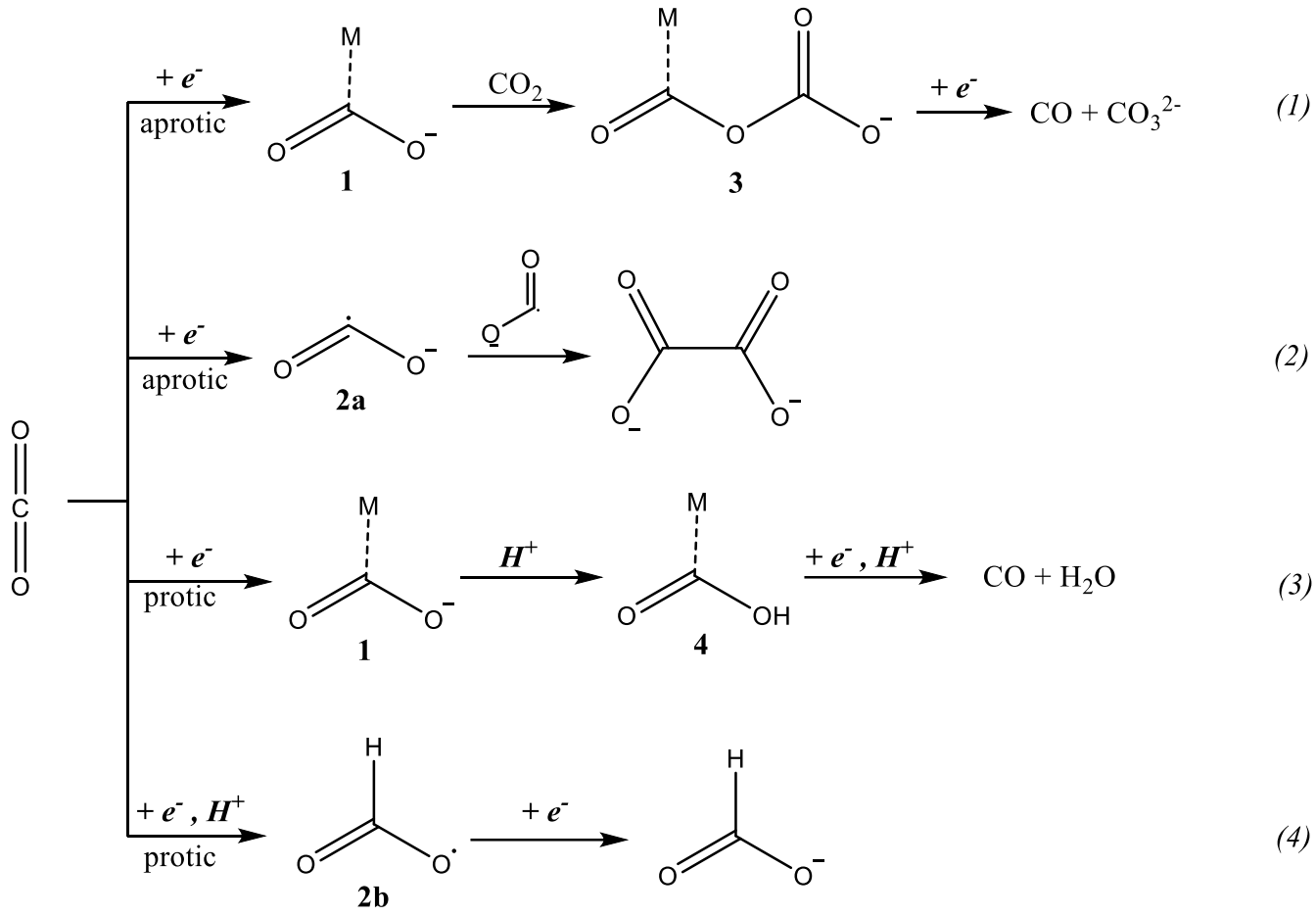

Figure 1.9: *Different mechanism of CO_2 reduction in different solvents (aprotic/aqueous) and using different electrodes*

CO, $HCOO^-$ and oxalate are not the only possible products, in fact they can be further reduced in H_2CO [19], CH_3OH[20][21], CH_4 and other hydrocarbons[22].

These reactions can be conducted by a semiconducting photocathode or by an electrode powered by PV devices. In the first case the light is absorbed by a semiconductor electrode or light harvesting particles which are absorbed or covered on the electrode surface. The absorbed photon caused a photoinduced electron transfer to catalyst, which can finally reduce CO_2. In the other case a voltage is applied in the electrode and then it can active CO_2. The main disadvantages of this technique are the use of high overpotentials and the poisoning and deactivation of the electrode surface. [15][23]

1.2.3.2 Homogeneous catalysis: photoactivated CO_2 reduction

One of the first homogeneous systems has been described from Lehn *et al.*[24]. Lehn and co-worker used a solution of $Ru(byp^{*2})^{2+}{}_3$, $CoCl_2$ (respectively as PS and cat) with CO_2 dissolved in a solution of CH_3CN/H_2O to produce CO/H_2 mixture under Xe lamp irradiation, several different amines have been tested as SED. The turnover numbers (TON*[3]) are 32 for $Ru(bpy)^{2+}$ and 9 for $CoCl_2$, the selectivity, expressed as CO/H_2 ratio, is strongly conditions dependent (from 0,02 to 24,9). After this paper, several transition metals have been tested to produce mainly CO, H_2 and $HCOO^-$ in different conditions with the intent to increase performance. The photoactivated reduction mechanism has been explained using $Re(bpy)(CO)_3Cl$. $Re(bpy)(CO)_3Cl$ absorbs light, an electron is promoted in the excited state by metal to ligand charge transfer (MLCT) process and intermediate **6** is produced; now intermediate **6** is able to oxidase a SED in SED^+. The intermediate **7** is in equilibrium with **8**, which can receive an H (from a hydrogen source) and produced hydride **9**. At this point, CO_2 can be coordinate from intermediate **9** and CO_2 reduction is catalysed by Re-complex. Then, $HCOO^-$ dissociates and intermediate **12** associates a Cl^- to regenerate the catalyst (Figure 1.10) [25].

Catalyst and photosensitizer can be the same molecule [25], two different and no-linked compounds[24] or two different metallic cores coordinated by the same polydentate ligand, but systems with bridging ligand show better performance than separated systems.[26] Several metals have been tested as catalyst to reduce CO_2, for example: Ni^{2+}, Fe, Re^+, Pd^{2+}, Ru^{2+}, Rh^{3+}, Co^{3+}; using mainly three class of ligands: phosphines, (di)imines and macrocylics .[27]

Another important variable is SED, since the first paper Lehn and co-worker has been tested four different amines as SED (triethanolamine, trimethylamine, triethylamine, tripropylamine). The effect of SED on CO/H_2 ratio has been evident: using triethanolamine the selectivity is 500 times higher than using trimethylamine. [24] Afterwards, numerous different compounds have been used as SED, for example aromatic amine, 1-benzyl-1,4-dihydronicotinamide (BNAH), 1,3-dimethyl-2-phenylbenzimidazolidene (BIH), ascorbic acid, carboxylic acids and thiols. Generally, amines have furnished the best outcomes, but the SED effect can easily change with conditions, PS and cat. Unfortunately, none of these SEDs can be used in an economic-sustainable artificial photosynthesis process. [28] Ideally, water is the sacrificial electron donor, as in natural photosynthesis.

With the intent of complete the description of the photoactivated CO_2 reduction mechanism, the oxidative mechanism of trimethylamine is described. The intermediate **6** reduce a trimethylamine

[*2] bpy:2,2[I]- bipyridine

[*3] TON: moles product/moles catalyst

(TEA) to produce **7** and the positive charge radical **13**, the radical **13** reacts with TEA to produce new radical **14** and the ammonium salt **15**. The radical **14** is the "proton source", which furnish an hydrogen atom at complex **8** to produce **9** and etenyldiethylamine.[25]

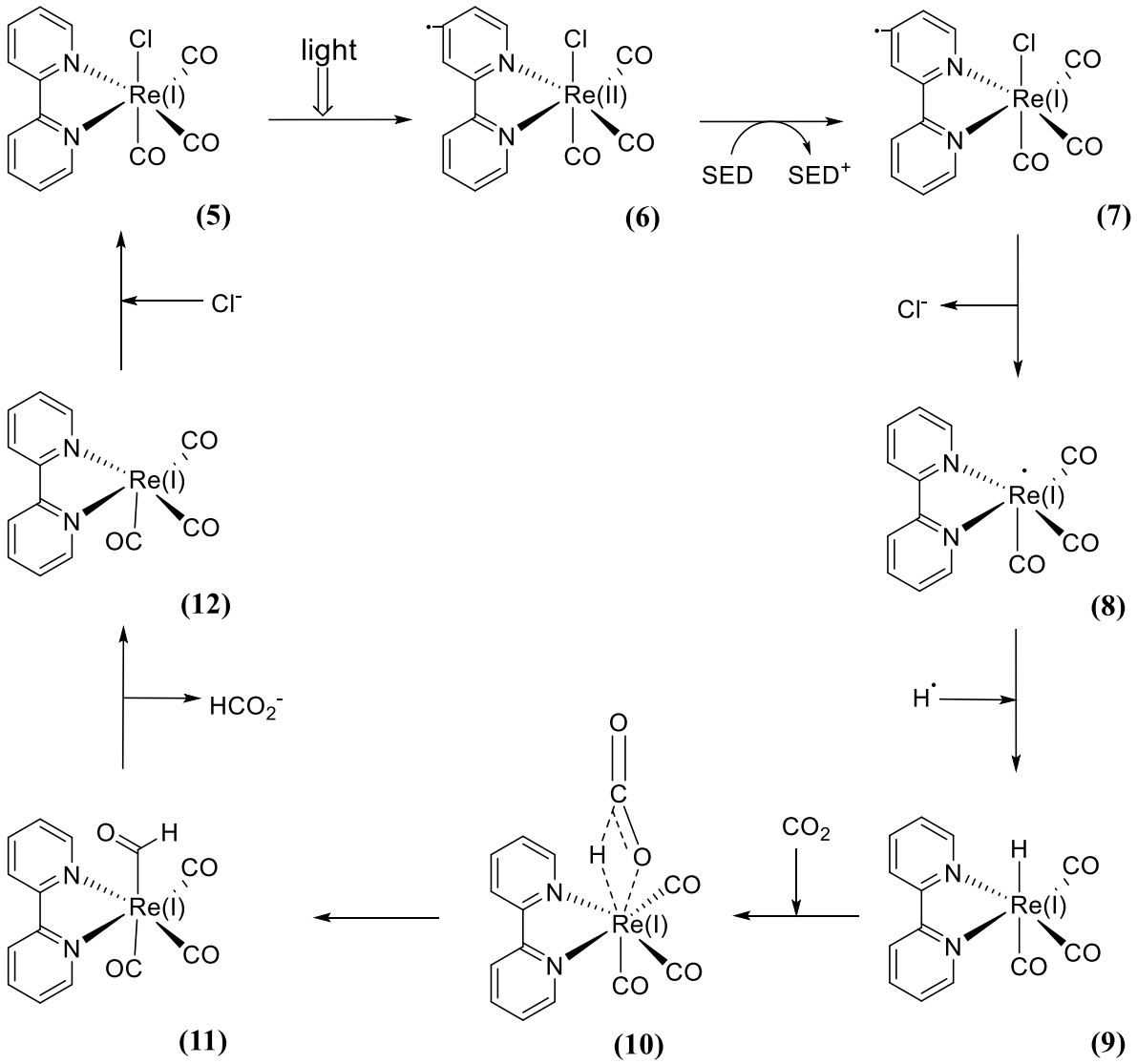

***Figure 1.10**: Photoactivated mechanism to reduce CO_2 catalysed by Rebyp(CO)$_3$Cl*

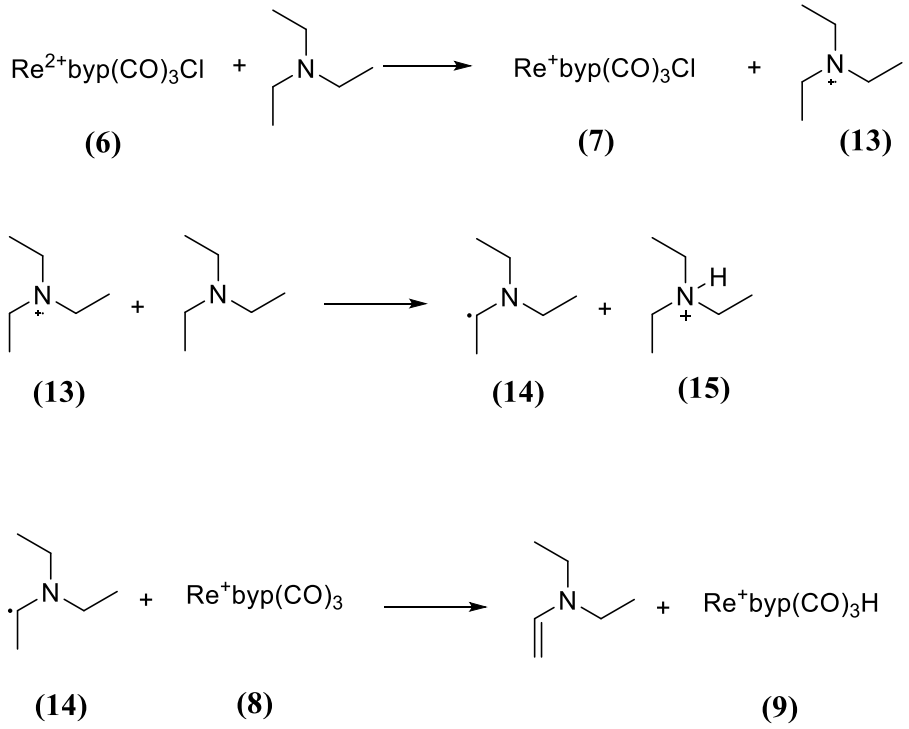

Fig 1.11: *Oxidative mechanism of triethylamine*

Nowadays, the new systems have TONs in the order of hundreds, but this parameter should grow up and also the stability of compounds have to increase. Compared to heterogeneous systems, homogeneous systems suffer from a big restriction. In fact, using metal complexes, it is often possible to transfer only 2 electrons (the limit is the oxidation state of metallic core). On the other hand the electrode surface have not this limitation, so it is possible reduce furtherly CO_2 in higher reduced compounds (up to CH_4).[29] Several of these systems use rare and expensive transition metals (especially for PS), but with the purpose of development and scale-up models, cost-effective and earth-abundant metals must substitute the rare metals in the new systems. [15]

1.3 Development of Cu(N^N)(P^P) based PS

A possible option is represented by Cu-based PS. Copper is cheaper and more abundant than Pd, Pt, Ir, Os, Rh and Ru (the estimated world reserves for Cu are 830 000 000 tonne against 100 000 tonne for all other metals).[30],[31] In solution, the most common Cu oxidation states are +2 and +1. Cu^{2+} complexes have d^9 configuration and a planar square geometry. In this kind of complexes are, also, observable d-d metal-metal centred transitions, which absorb radiations in the visible spectral window and produce ultrafast non-radiative deactivation process. So, Cu^{2+} excited states have very short lifetime and it is not possible to used them as PS. On the other hand, Cu^{+} complexes have d^{10} configurations and a tetrahedral geometry. In this case the d-d metal-metal centred transition is not observable, the electron can be excited from d metal orbitals to π^* ligand orbitals by MLCT or from π ligand orbitals to π^* ligand orbitals. Cu^{+} complexes absorb light in UV-Visible window and have a higher time life than relatives Cu^{2+} complexes.[32] After light promoted excitation, Cu^{+} complexes became formally Cu^{2+} and the geometry of the excited state changes from tetrahedral to similar square-based pyramid by a pseudo Jahn-Teller distortion (PJT) (Figure 1.12). Now, a nucleophilic species (as solvents) can react with metal centre and quench the MLCT, causing shorter time life of excited state. This process can be reduced and using ligand with bulky substituents. [33][34]

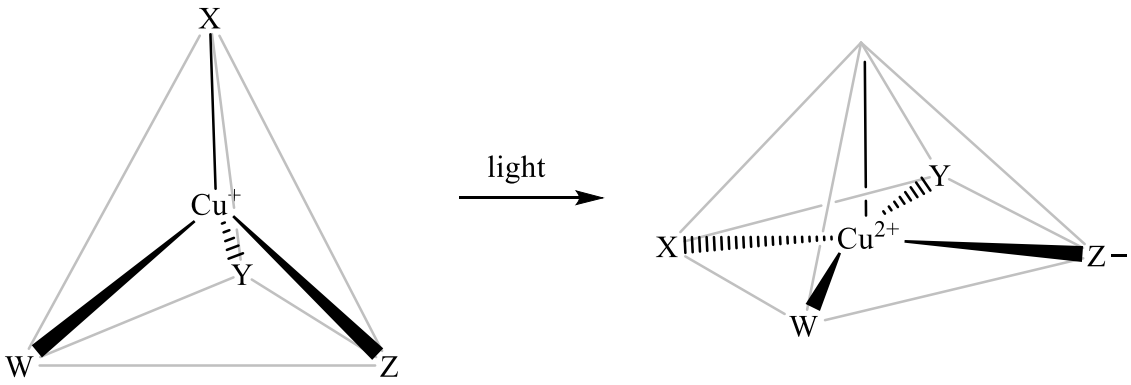

Figure 1.12 *Cu^{+} absorbs a photons and has a MLCT, the consequence is a molecular shape change from tetrahedral to pseudo square-based pyramid. The excited state can be quenched by exciplex quenching*

Chelating phosphines with high sterical hindrance are a good choice. In fact, it has been demonstrated that the use of these ligands can increase the lifetime of the excited states in Cu^{+} complexes. In addition, the use of chelating ligands could suppress ligand dissociation, with an additional lifetime increasing. Several different phosphines have been studied, but one of the best options is bis[2-[(diphenylphosphino)phenyl]ether (POP) (Figure 1.13). [35][36]

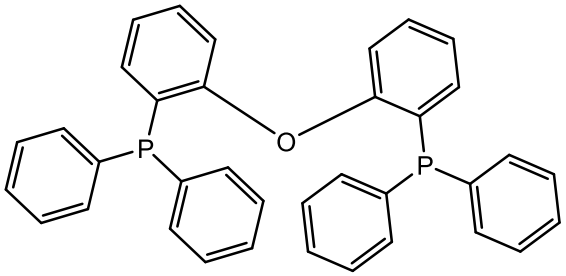

Figure 1.13 *bis[2-[(diphenylphosphino)phenyl]ether (POP)*

Another category has been studied to realize Cu^+ complexes: diimine bidentate ligand (N^N). Even in this case, a chelating ligand could reduce ligand dissociation and it is possible reduce the exciplex quenching process using bulkier lateral chains. The steric hindrance of lateral chains can be used also to favour the heteroleptic Cu complexes.[37] In fact McMillin *et al.* have studied Cu(I) complexes prepared from 1,10-phenanthroline derivatives and POP and they have discovered that these kind of complexes show long lived MLCT excited states,[38] afterwards numerous Cu^+(N^N)(P^P) complexes has been developed, obtaining impressive performance. These molecules can absorb light in two different regions of the spectral window: UV and visible.

The UV absorption bands (with extinction coefficient ε between 10^4 and 10^5 M^{-1} cm^{-1}) is assigned to π-π^* ligand transitions centred; the electron is excited from ground state to π-π^* intraligand charge transfert (^{1}ILCT), which can change its spin multiplicity to produce ^{3}ILCT by an intersystem crossing process (ISC). The second band is centred at around 300 nm (with ε between 2×10^3 and 4×10^4 M^{-1} cm^{-1}) is assigned to MLCT transitions. The electron is excited from the ground state to ^{1}MLCT, subsequently, by a PJT, the excited state can pass from a pseudo tetrahedral to pseudo planar square geometry ($^1MLCT_{flattened}$ state), this process can be inhibited using the right ligand. The $^1MLCT_{flattened}$ state can interconvert in ^{3}MLCT state by ISC process. Both ISC processes are favoured by symmetry of the complex. Excited states return to ground state by thermal or luminescent processes.[39] (Figure 1.14)

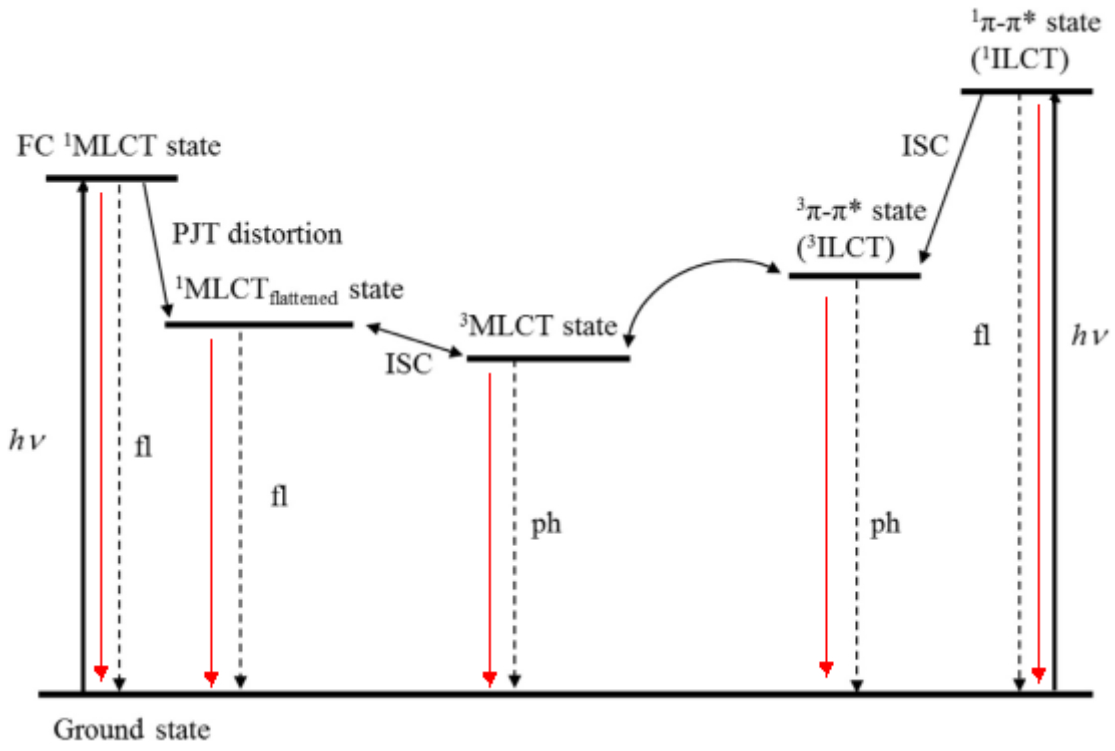

***Figure 1.14**: Jablonski diagram for Cu(N^N)(P^P) complexes. The black arrows represent light excitation process, the dashed arrows represent de-excitation luminescent processes: fluorescence (fl), phosphorescence (ph), the red arrows represent de-excitation thermal processes*

A useful PS has to show the following properties: visible light absorption, long-living excited state lifetime (close to 1 µs) and be photostable. [40] Recently, Cu^+(N^N)(P^P) complexes have been generating interest because some of these compounds show excited state lifetime in the order of 1 µs and absorption band in the visible range. [39] With the intent of discover new and higher-performance PS, several N^N ligand are studied and tested, among them, the most used are 1,10-phenanthroline derivatives. However, other N-containing heterocycles have been under investigation.

1.3 Substituted 1,2,3-triazoles as N^N ligand

Heterocycles as 1,2,3-triazole can be easily synthesized by azides and ethynyl derivatives by 1,3-Huisgen cycloaddition.[41] More recently, one of the so-called click-reaction, Cu-azide-alkyne-catalyzed reaction (CuAAC), discovered by Barry Sharpless, is one of the most used technique in order to form 1,4-disubstituted-1,2,3-triazoles.[42] Using this synthetic pathway, it is possible obtain the desired product with high selectivity and high yield from organic azides and acetylene

derivatives. Organic azides can be commercially available or synthesized by nucleophilic substitution; in any case they must be carefully handled, because the azide group can easily decompose, releasing N_2 and generating explosions[43]. Acetylene derivatives are also commercially available or can be synthesized by Pd-catalysed coupling.[44] Bizzarri and co-workers synthesized and studied three different Cu^+(N^N)(POP) using 4,5 disubstituted triazoles as N^N. In particular, they used 5-(6'-methyl--pyrid-2'-yl)-4-phenyl-1*H*-1,2,3-triazole and two derivatives of this ligand. Compound **16** is the mononuclear complex produced with the simplest triazole, **17** and **18** are dinuclear complexes produced using two "pyridyl-triazole unit" linked by a phenyl bridge (the two substituents are respectively orientated in *meta* and *para* positions) (Figure 1.15)

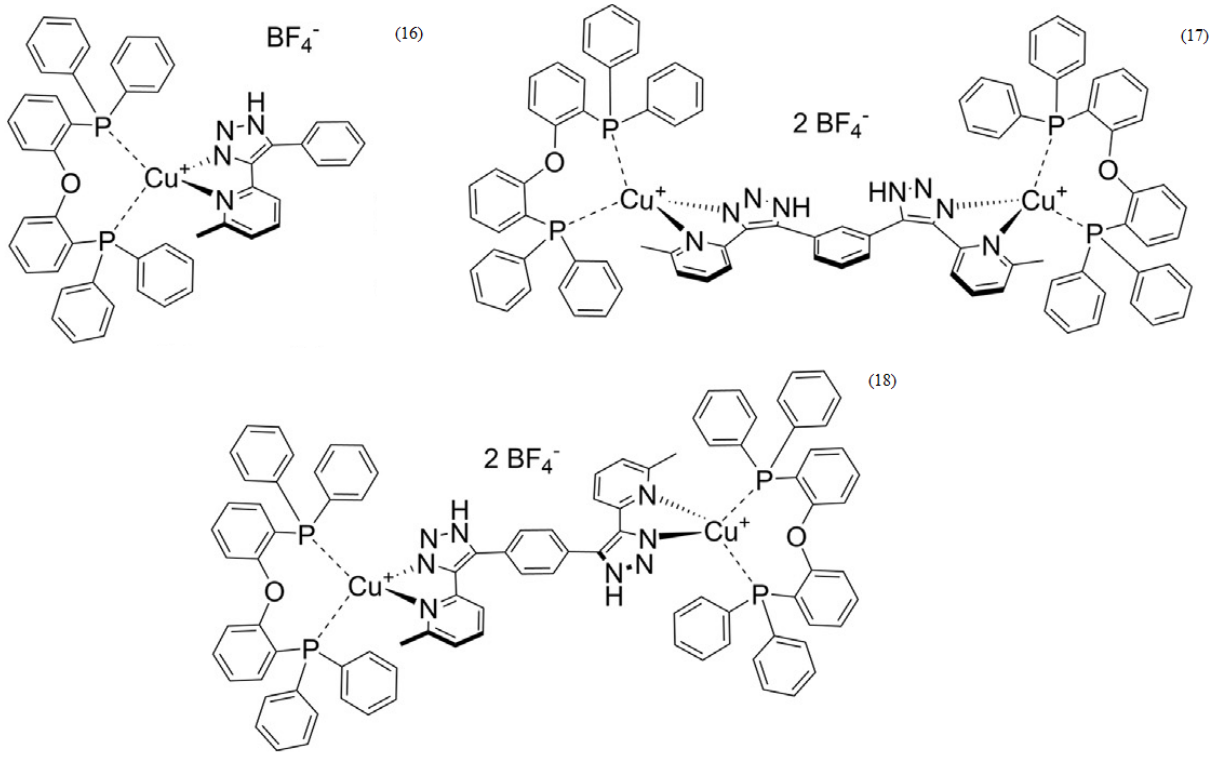

Figure 1.15 *Heteroleptic Cu^+ complexes synthesized by Bizzarri.* [45]

These complexes showed very interesting and motivating outcomes. They absorb light until 400 nm and the excited state life times are 0,88 μs **(16)**, 1,21 μs **(17)**, 2,78 μs **(18)**. In addition, a second metal centre could positively influence the excited state lifetime and this effect can be mediated by π-conjugated system (as the phenyl ring). In the end, they confirmed the importance of sterical hindrance to improve the excited state lifetime, in fact the presence of methyl group in αposition to the N of the pyridine has a positive response.[45]

The photophysical and electronic properties of these complexes were promising for their use as PS in photochemical CO_2 reduction. However, their lack of absorption in the visible range would be a problem in view of a real application with solar irradiation. Therefore, different substituents have

been under investigation, in particular using quinoline ring instead of pyridine. Recently, three different 1,4-disubstituted triazole, with a quinoline as substituent, have been synthesized and tested.

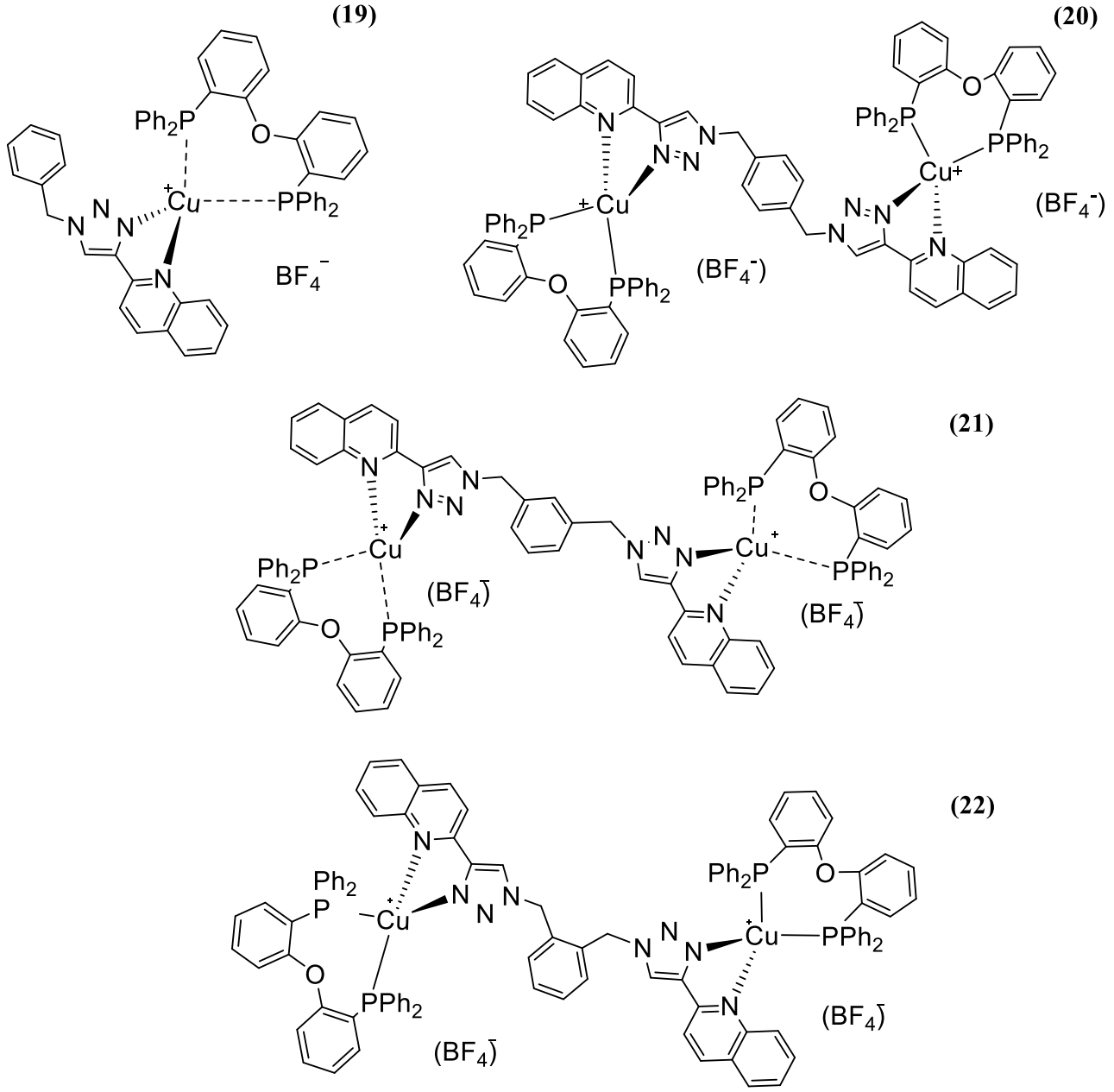

Figure 1.16: *Cu(N^N)(POP) ligands synthesized by Bizzarri and co-workers, these ligands have a quinoline as substituent to improve the light absorption.*[46]

Compared to complexes **16, 17** and **18,** the complexes in Figure 1.16 can absorb light in a wider spectral window (until 450 nm).[46] In fact, quinoline as a higher π-conjugation in respect to the pyridine so that the LUMO of the final heteroleptic Cu complex is more stabilized, allowing blue-light absorption of the ^{1}MLCT. Motivated by these results, we investigate further these particular ligands and the complexes thereof.

2 AIM OF MY THESIS

The interesting results obtained in the last years are stimulating the study of triazole derivatives as diimine chelating ligands in heteroleptic Cu^+ used as photosensitizer. Using these ligands, the heteroleptic Cu^+ complexes have showed excited state life times in the order of μs, satisfying one of requirement to be a photosensitizer. Another important feature to be a good photosensitizer is the capacity of absorb light in the visible spectra. Several complexes absorb light until 400 nm, but using quinoline as substituent it is possible absorb light until 450 nm

In view of encouraging data, the aim of my thesis has been the synthesis and the characterization of derivatives of 1,4-disubstituted-1,2,3-triazoles and their use as ligand in heteroleptic Cu^+ complexes, to produce mono-, di-, tri nuclear systems. The synthesis of these ligands can occur in few steps and a large part of these steps can be classified as green chemistry reactions. With the purpose to increase the absorption in the visible region, 2-quinolin derivatives are used.

3 RESULTS AND DISCUSSION

My project can be divided in the following steps:

1. Synthesis 1,4-disubstituted-1,2,3 triazole derivatives (**23**, **24**, **25**, **26**, **27**)

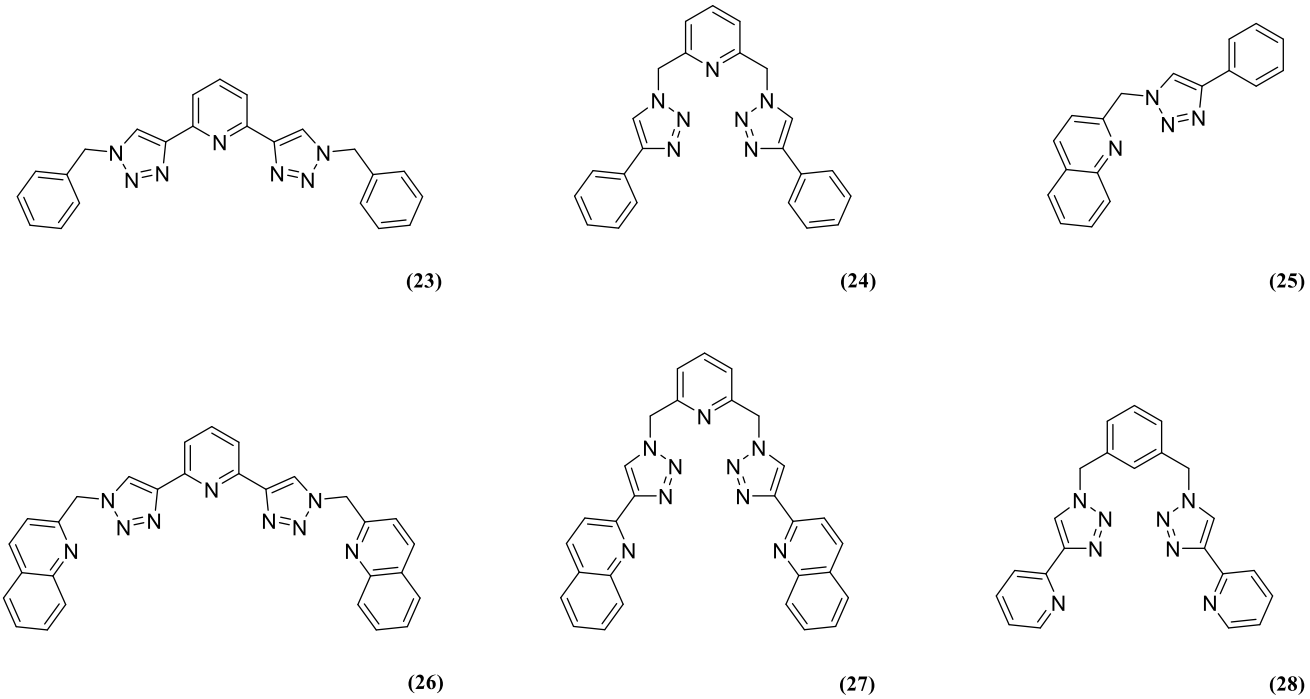

(23) **(24)** **(25)**

(26) **(27)** **(28)**

Figure 3.1*: Structures of ligands **23**, **24**, **25**, **26**, **27**, **28***

2. Synthesis of mono-, di-, tri- nuclear heteroleptic Cu^{+} complexes from ligand **23**, **24**, **25**, **26**, **27**, **28** and triphenylphospine (PPh_3) or bis[2-[(diphenylphosphino)phenyl]ether

3. Ligands and complexes are characterized by ^{1}H-NMR, ^{13}C-NMR and, if it is possible by X-ray

4. The following proprieties of ligands and complexes are studied: redox potentials (evaluated by cyclic voltammetry), absorptivity coefficient, absorption and emission (by UV-Visible spectrophotometry and spectrofluorimetry).

3.1 Synthesis of ligands

3.1.1 Synthesis of 2,6-bis(1'-benzyl-1',2',3'-triazol-4'-yl)pyridine (**23**)

The first step is a Sonogashira-coupling between 2,6-dibromopyridine (**29**) and two equivalents of trimethylsilylacetylene (**30**), the product is the intermediate **31** (Y=52%). $Pd(Ph_3)_4$ and CuI are, respectively, catalyst and co-catalyst [44], a dry mixture of diisopropilamine (DIPA) and toluene is used as solvent, the reaction is conducted in inert atmosphere. Instead of $Pd(Ph_3)_4$, $Pd(Ph_3)_2Cl_2$ has been tested, obtaining lower yields (37%).

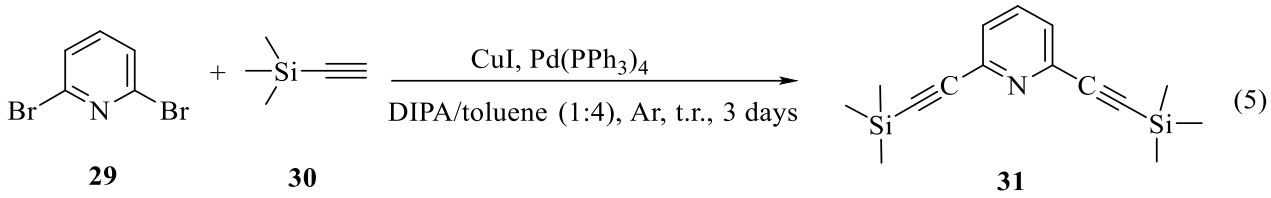

***Figure 3.2**: Synthesis of 2,6-bis((trimethylsilyl)ethynyl)pyridine (**31**)*

Trimethylsilyl group is indispensable, because it prevents the double C-C coupling of acetylene in the previous step. Thus, it has to be removed to proceed with synthesis. The following step is the deprotection of alkyl functionality using K_2CO_3 dissolved in methanol (MeOH). The intermediate **32** can easily degrade at room temperature.

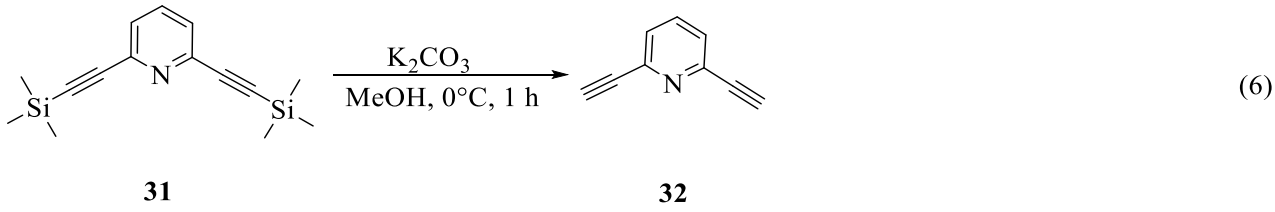

***Figure 3.3**: Synthesis of 2,6-biethynylpyridine (**32**)*

The last reaction is a Cu-catalysed Azide Alkyne cycloaddition (CuAAC) between intermediates **32** and benzyl azide (**33**). The ligand ***23*** is obtained with a yield of 83%.

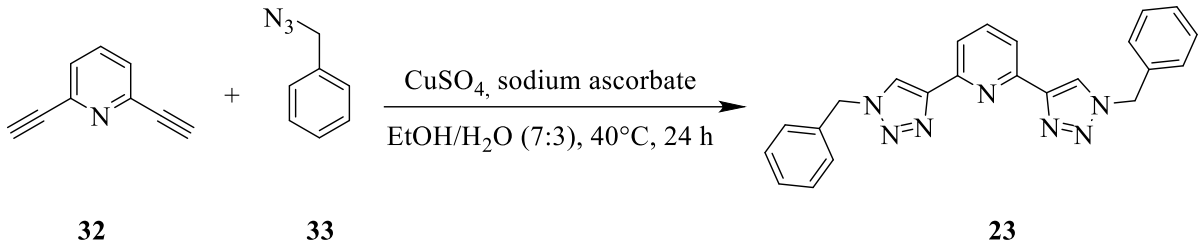

(7)

32 **33** **23**

Figure 3.4**: Synthesis of ligand **23

3.1.2 Synthesis of 2,6-bis((4'-phenyl-1',2',3'-triazol-1'-yl)methyl)pyridine (**24**)

The ligand **24** can be easily produced in a one-pot reaction (Y= 60%). The organo-azide species is generated *in-situ* by nucleophilic substitution (S_N2) between NaN_3 and 2,6-dibromomethylpirydine (**34**), where the NaN_3 is the nucleophilic specie. Afterwards, CuAAC reaction can occur between organic-azides and ethynilbenzene (**35**).

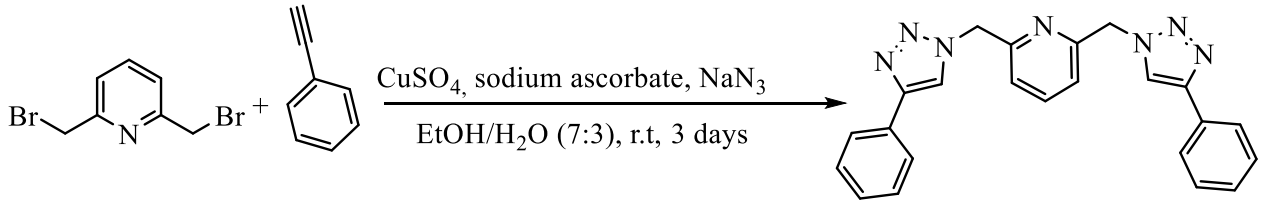

34 **35** **24**

Figure 3.5**: Synthesis of ligand **24

3.1.3 Synthesis of 1(2-methylquinolinyl)-4-phenyl-1,2,3-triazole (**25**)

The first step is a bromination of the methyl group in quinaldine (**36**). This reaction occurs by a radical process, where N-bromidesuccinamide (NBS) is the "Br source" and benzoyl peroxide $(PhCO_2)_2$ is the termoactivated radical initiator.[44] This reaction is affected of several by-reactions, in fact poly-bromination reactions can easily promoted, increasing the reaction time. The reaction was conducted at reflux in acetonitrile (ACN) for 13 h and the yield was 49%, with increase of time to 25 h the yield of the desired product decreases to 14% (dibromomethylquinoline was produced with a yield of 26%).

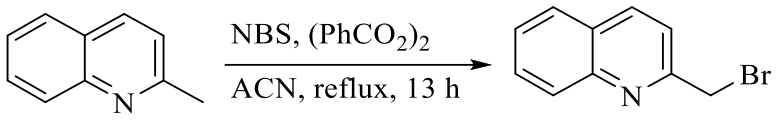

(9)

36 **37**

***Figure 3.6**: Synthesis of 2-bromomethylquinoline (**37**)*

The second step is a CuAAC between 2-azidomethylquinoline generate *in-situ* from 2-bromomethylquinoline (**37**) and ethynilbenzene (**35**), (Yield=63%).

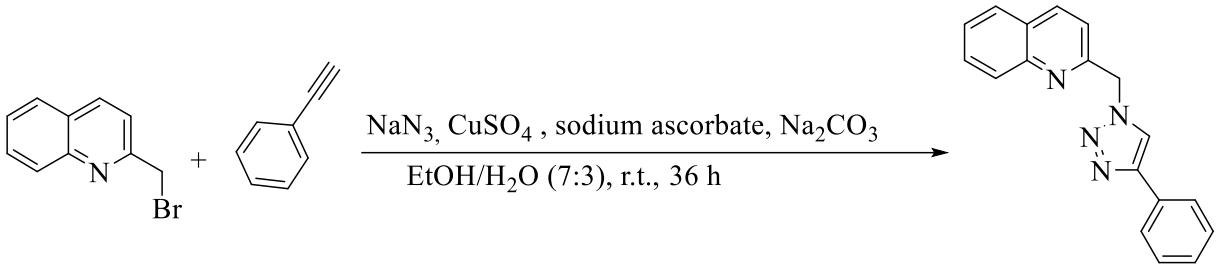

(10)

37 **35** **25**

Figure 3.7**: Synthesis of ligand **25

Another new and interesting synthetic pathway to produce ligand **25** has been tested. Brandhofer *et al.* have reported a one-pot reaction to produce triazole from an aliphatic group.[47] In the first step, a methylic C-H bond in **36** is substituted by C-azide bond. The second step is a CuAAC reaction. In the first step *tert*-butanolhydroperoxide (*t*-BuOOH), trimethylsilyl azide ($TMSN_3$), CH_3CN were added, after 2 h sodium ascorbate, diisopropylethylamine (DIPEA), *tert*-butanol (*t*-BuOH) were added. Unfortunately, this method did not give the expected result, in fact, the starting material **36** did not react.

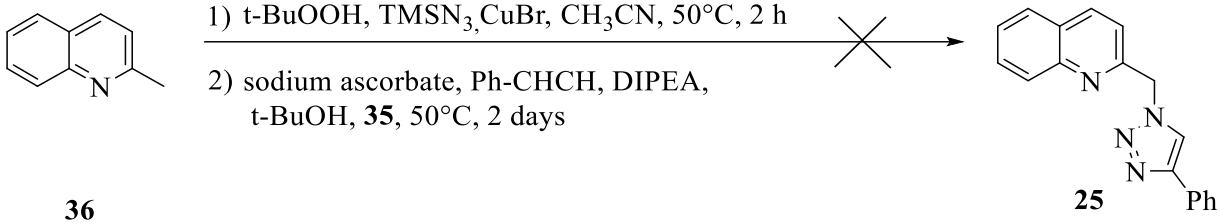

(11)

36 **25**

Figure 3.8**: Unsuccessful synthesis of ligand **25

3.1.4 Synthesis of 2,6-bis(1'(2''-methylquinolinyl)-1',2',3'-triazol-4'-yl)pyridine (**26**)

The intermediated **31** is produced as in reaction *5* and the intermediated **37** is produced as in reaction *9*. With the purpose of avoid the degradation of **32**, a one-pot reaction has been tested. Where the first reaction is a deprotection of acetylene group (the reaction *12a* is similar at reaction *6*, the only difference is the solvent). The second step is a standard CuAAC. The yield is 67%, so it is a discrete yield, nevertheless it should be possible to improve using optimised conditions.

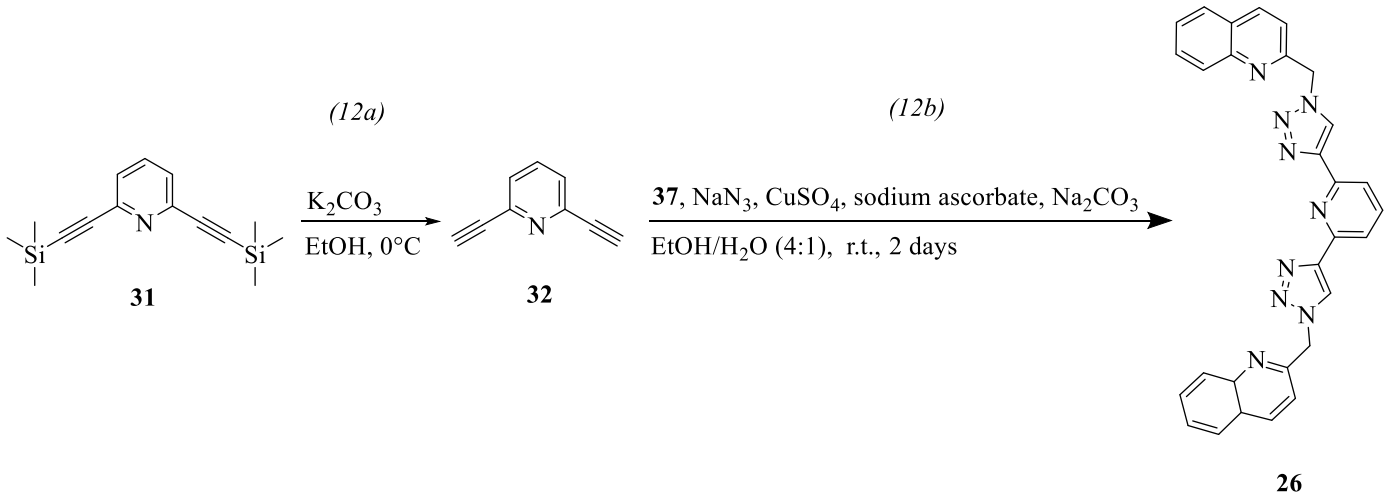

Figure 3.9**: One-pot synthesis of ligand **26

3.1.5 Synthesis of 2,6-bis((4'-quinolin-2''-yl-1',2',3'-triazol-1'-yl)methyl)pyridine (**27**)

The intermediate **39** is synthesized by a Sonogashira cross-coupling reaction between 2-bromo-pyridine (**38**) and trimethylsilane (**30**) (Y=16%)

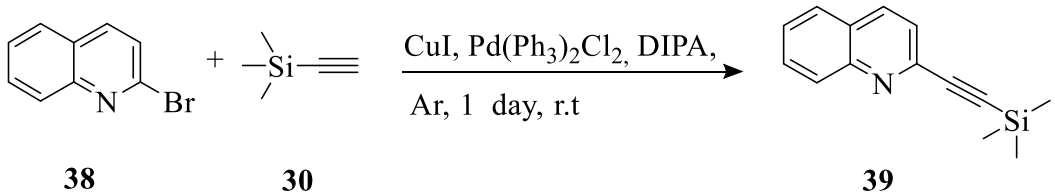

(13)

***Figure 3.10**: Synthesis of 2-(trimethylsilylethynyl)quinoline (**39**)*

With the purpose to avoid the degradation of **40**, a one-pot reaction has been tested: the first reaction is a deptrotection of the acetylene group, the second step is a standard CuAAC. The overall yield is 34%.

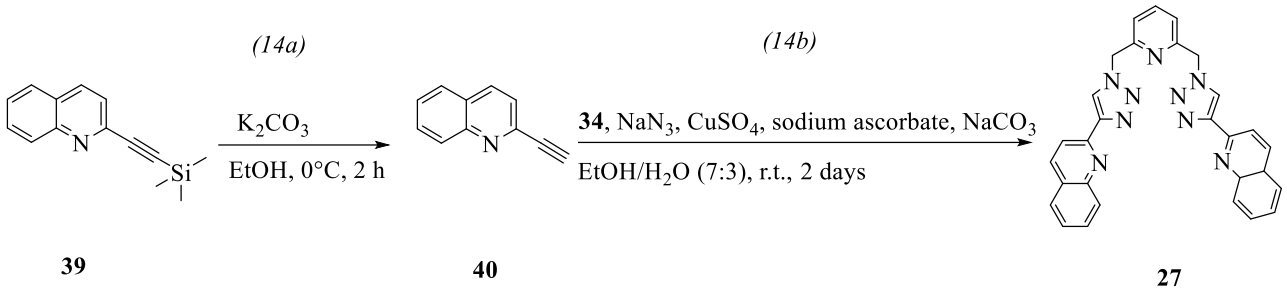

Figure 3.11**: One-pot synthesis of ligand **27

3.2 Synthesis of heteroleptic Cu^+ complexes

Heteroleptic Cu^+ complexes can be easily produced with the following procedure, independently of ligands. $Cu(CH_3CN)_4BF_4$ (**41**) and phospine (PPh_3 or POP) are dissolved in dry dicloromethane (DCM) to produce the first intermediate (**42** o **43**), where one or two molecules of CH_3CN are substituted by (di)phospine. Then the diimine ligand (N^N) or triimine ligand (N^N^N) is added, and chelate the Cu+ ion, producing the heteroleptic Cu^+ complex. Yields are collected in Table 3.1

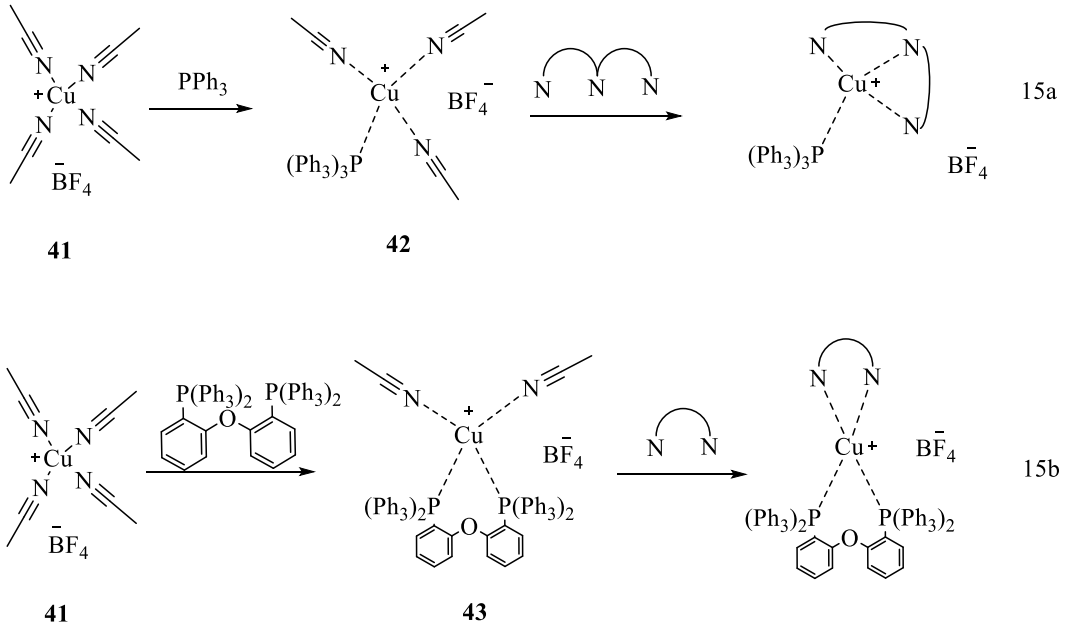

***Figure 3.12**: Generic synthesis for heteroleptic Cu^+ based complexes*

Complex	Yield (%)	Ligand	Number of coordinated Cu^+	Phospine
44	86	**23**	1	PPh_3
45	69	**24**	1	PPh_3
46	/	**25**	1	POP
47	91	**26**	3	POP
48	35	**27**	3	POP
49	100	**28**	2	POP

***Table 3.1**: Summary table about yields and structures of complexes*

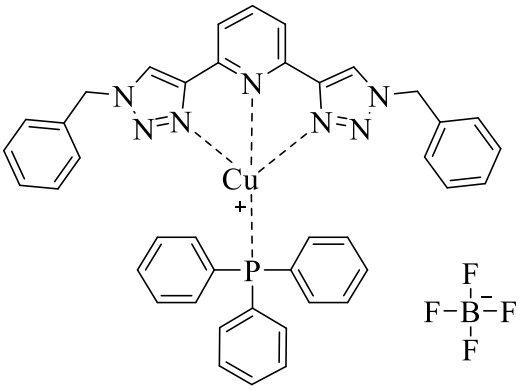

44

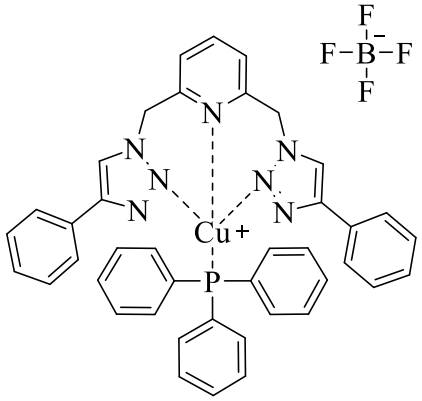

45

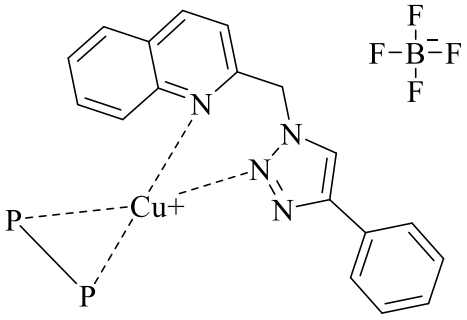

46

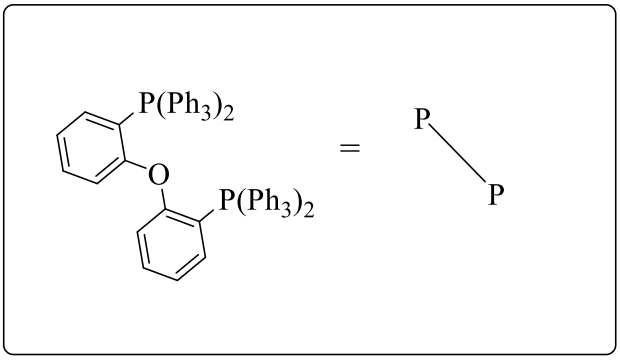

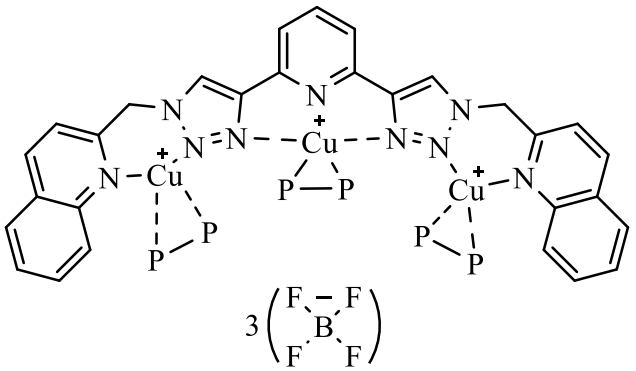

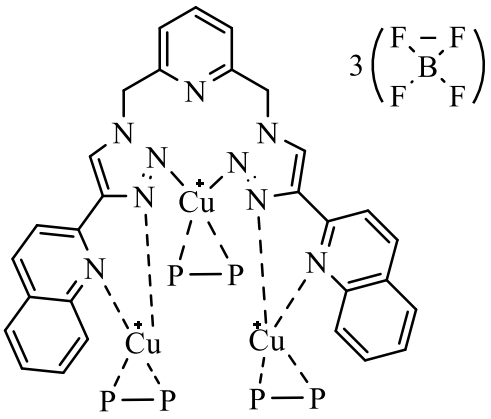

47 **48**

***Figure 3.13a**: Structure for heteroleptic Cu-based complexes (**44**, **45**, **46**, **47**, **48**)*

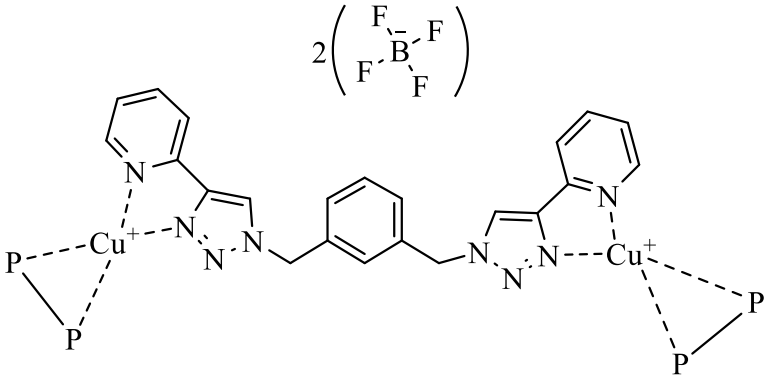

49

***Figure 3.13b**: Structure for heteroleptic Cu-based complex (**49**)*

3.3 Structure characterization of ligands and complexes

All ligands and complexes are characterized using ^{1}H-NMR and ^{13}C-NMR. For complex **44** it is also available the X-ray structure. All data are collected in Chapter 5.

3.4 Photophysical data

All solid samples are dissolved in spectroscopic dicloromethane (DCM), analysis are conducted in quartz cuvettes, at room temperature and, only for complexes, under Ar atmosphere.

3.4.1 Determination of absorptivity coefficient (ε)

Three solutions at different concentrations were done for each compound (between 5 µM and 50 µM). Absorbance (A) has been measured from 230 nm to 800 nm (increment of 1,0 nm), then, using Beer law ($\varepsilon(\lambda) = \frac{A}{b \times C}$,where c is the concentration of the sample and b is the light path-length of the cuvette, equal to 1 cm). The reported ε(λ) is the average of ε(λ) calculated with the previous equation at different concentration.

Ligands **23** and **24** are tridentate ligands with very similar structure: the first one has two 1-benzyl-1,2,3-triazoles bridged by a 2',6'-pyridine in position 4 and the second one has two 4-phenyl-1,2,3-triazoles bridged by a 2,6'-dimethylpyridine. They are isomers. However, their spectra are quite different. In fact, while ligand **24** has a maximum absorption at 250 nm, ligand **23** presents a second band with relative maximum at 300 nm. This might be due to an extended conjugation of the pyridyl-bridging ring. When the phenyl ring is substituted by a quinolone, the ter-chelating ligands **26** and **27** are formed, which are isomers between each other. Their absorption is at longer wavelength when comparing ligand **24** and **27**. This difference is caused mainly by the presence of quinoline that has a higher π-conjugation in respect to the phenyl. Both spectra of **24** and **27** exhibit similar peaks in the high energy region (λ_{max}(**24**)= 249 nm, λ_{max}(**27**)= 257 nm) with similar shape, it is should attributable to the pyridyl-triazole system. In spectrum of **24,** no signals are visible over 290 nm. Instead ligand **27** absorbs light until 350 nm. Compared by ligands reported in literature (**16**, **17**, **18**) [45] there are not significant difference, except for a peak present under 260 nm in spectra **26** and **27**. In fact, these two compounds show a higher absorptivity coefficient in this part of spectra ($\varepsilon_{231\ nm}$(**26**) = 8,4 × 10^4 M^{-1} × cm^{-1}, $\varepsilon_{257\ nm}$(**27**) = 6,7 × 10^4 M^{-1} × cm^{-1} compared with $\varepsilon_{250\ nm}$ (**17**) = 2,2 × 10^4 M^{-1} × cm^{-1})

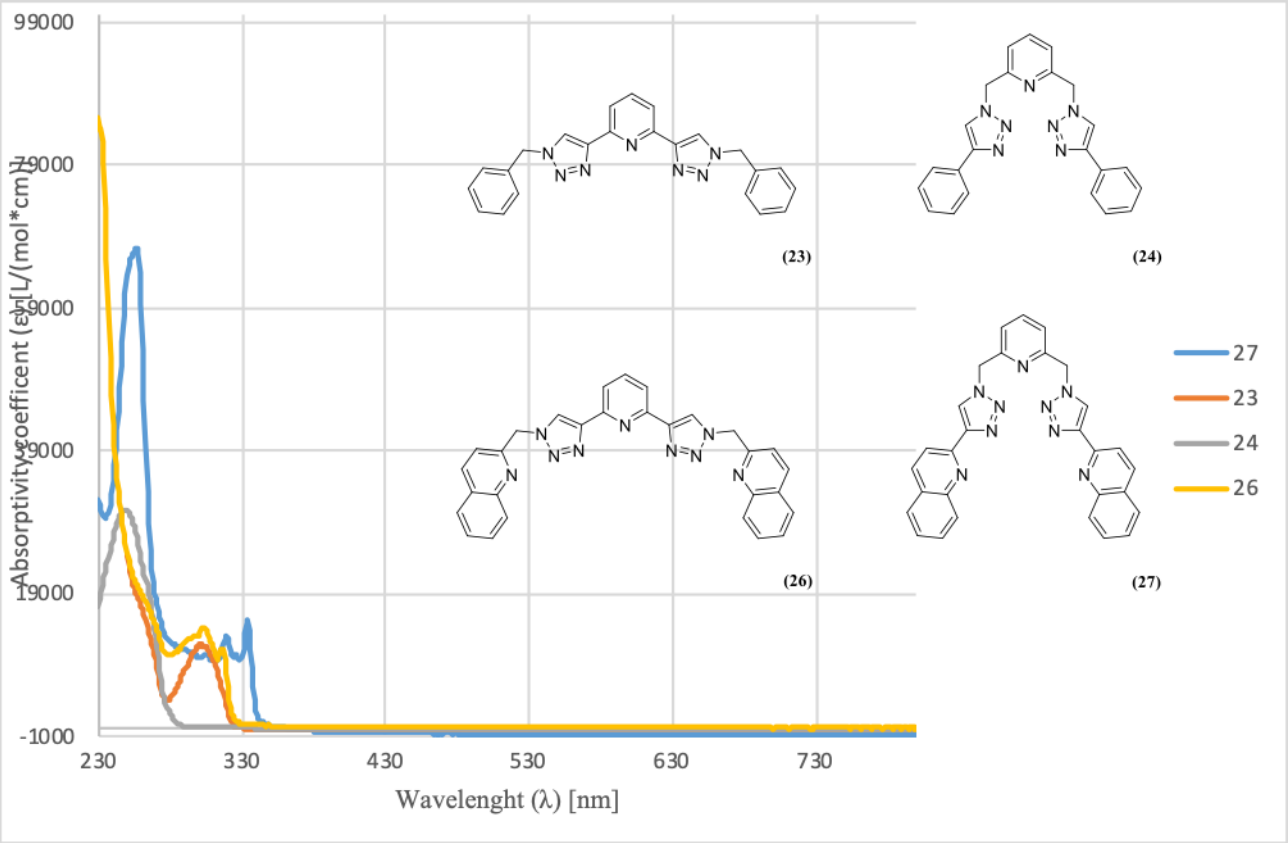

Figure 3.14: *Collected UV-visible absorption spectra of ligands (**23**, **24**, **26**, **27**)*

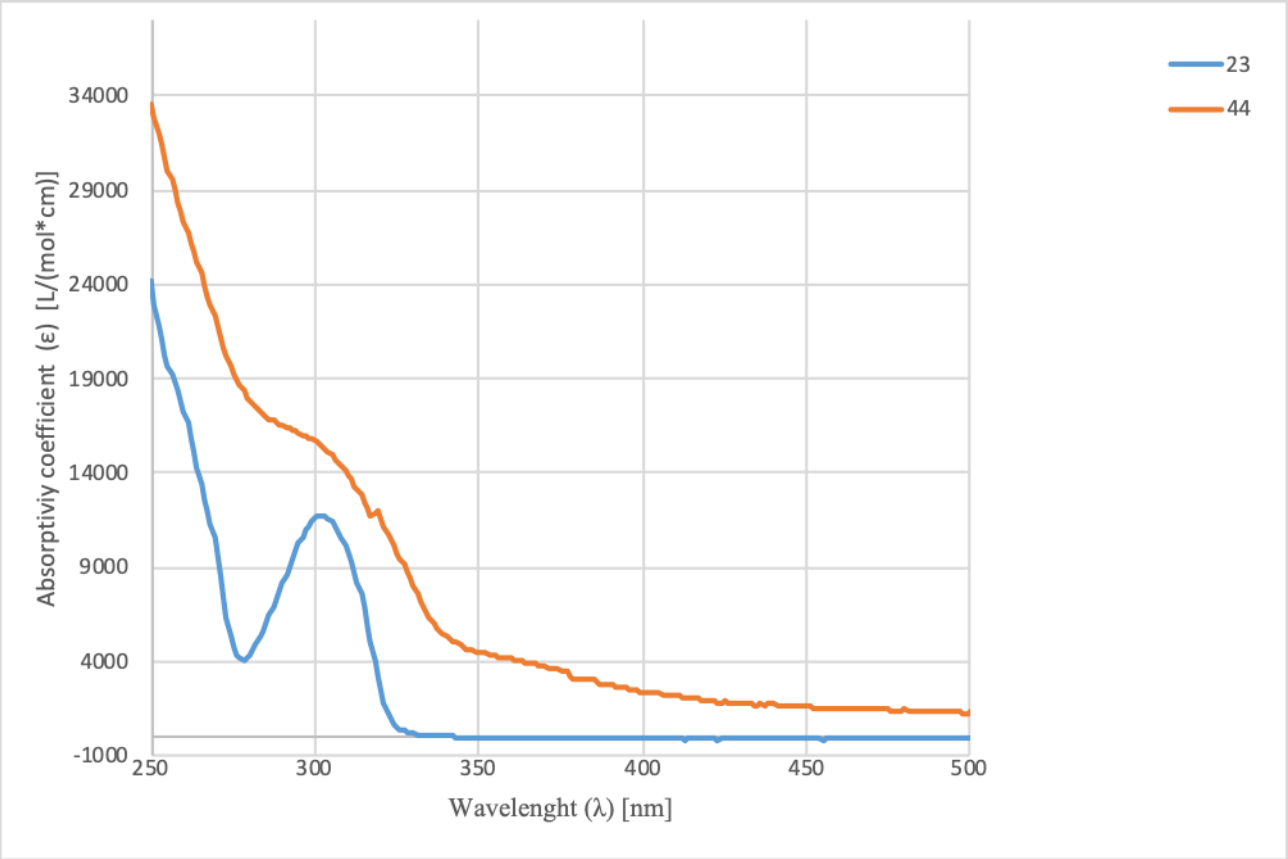

Figure 3.15a: *Compared spectra for ligand* ***23*** *and complex* ***45***

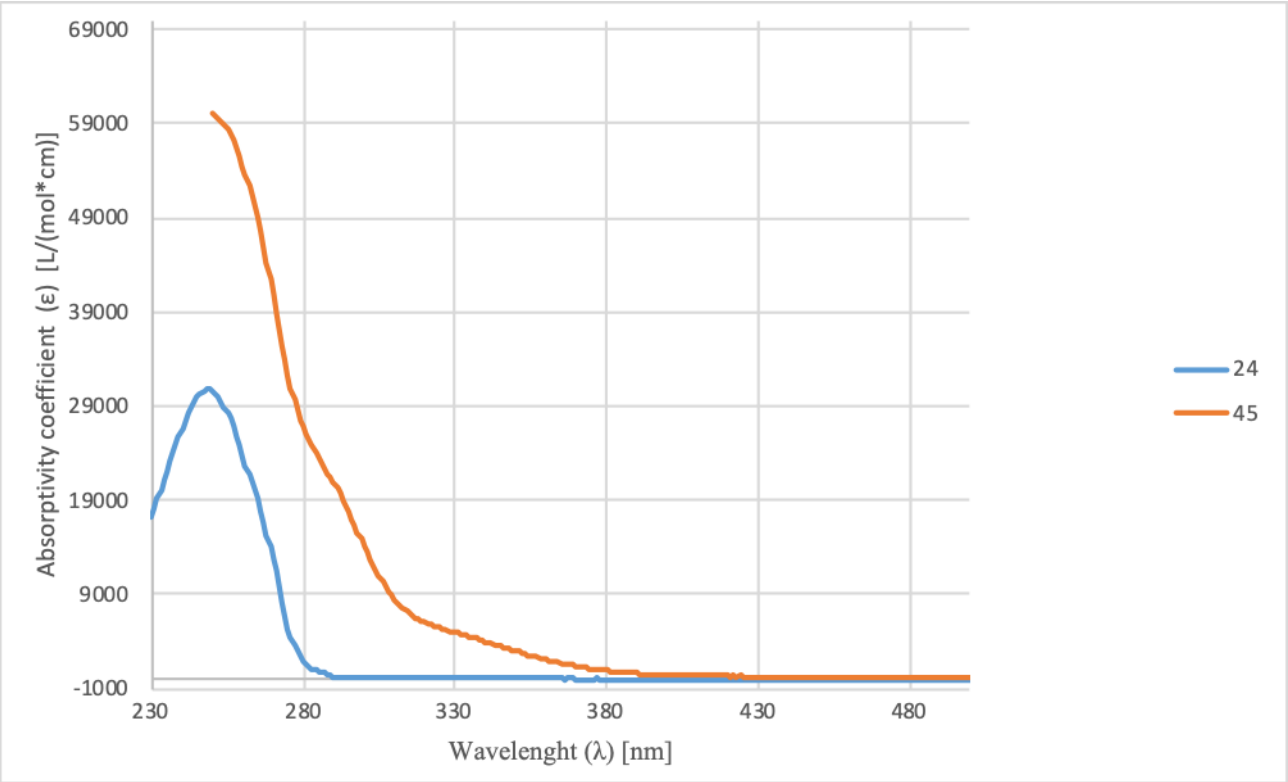

Figure 3.15b: *Compared spectra for ligand* ***24*** *and complex* ***45***

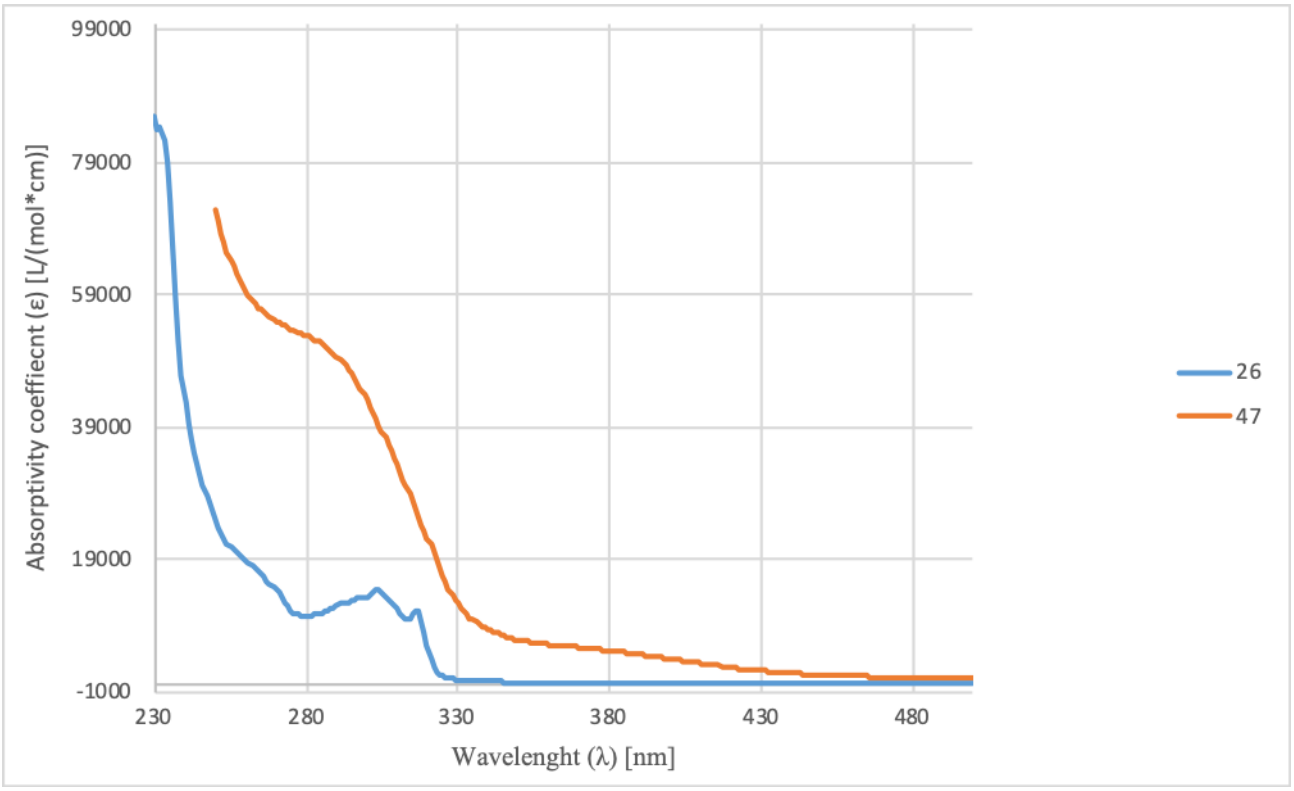

Figure 3.15c: *Compared spectra for ligand* ***26*** *and complex* ***47***

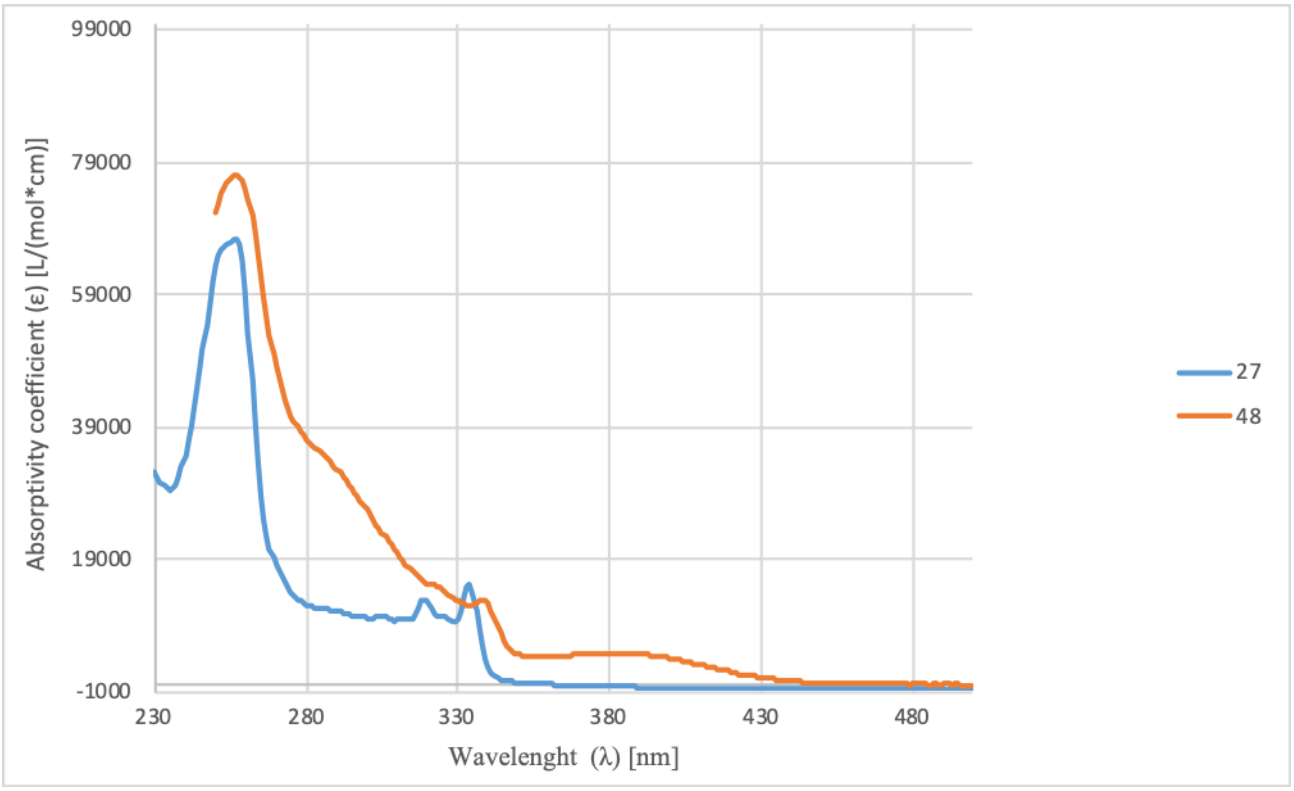

Figure 3.15d: *Compared spectra for ligand* ***27*** *and complex* ***48***

All heteroleptic Cu^+ complexes show high absorptivity coefficient between 250 nm and 350 nm. These absorptions are caused by π-π* and n-π* intra-ligand transitions centred on the phosphines and N^N (or N^N^N). Comparing heteroleptic complexes with relative ligands it is possible see an additional absorption region between 300 nm and 400/450 nm, so complexes can absorb light at lower energy than ligands. This band is attributable to ^{1}MLCT **44**, **45** and **49** absorb light until 400 nm, while **47** and **48** absorb light up to 450 nm. All these absorptions are caused by ^{1}MLCT from d metal orbital to π* ligand orbitals, but the different range is the result of different π-conjugates substituents (quinolinyl compared to pyridinyl or phenyl).

The presence of three and two coordinate centres are easily visible comparison **48** and **49** with **44.** In **48** and **49** ε are three and two times higher than **44**. No evident cooperativity effect is present in complexes **47**, **48**, **49**. **47** and **48,** which show very similar spectra to **19**, **20**, **21**, **22**[46].

In this discussion phosphines effect are not considered, because it was demonstrated that different phosphines as ligands can shift the spectra only few nm [37].

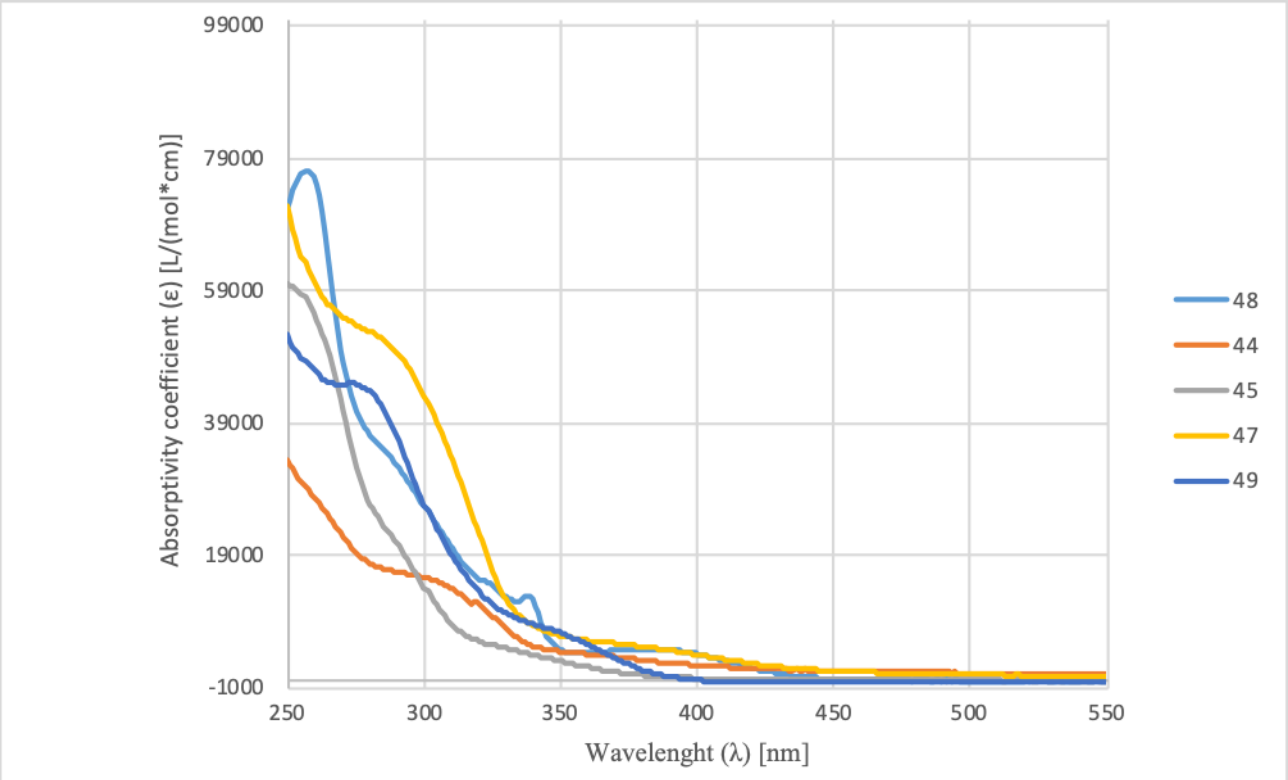

Figure 3.2: *Collected UV-visible absorption spectra of complexes (**44**, **45**, **47**, **48**, **49**)*

3.4.2 Analysis of emission and excitation spectra

The analysed solutions have a concentration between 25 µM and 50 µM. Ligand **24** has not shown emission properties. Ligands **26** compared with **23**, are affected by red-shift (figure 3.3). Another time, it is a consequence of different lateral chains. In fact, quinoline have higher π-conjugates system, which reduce the energy of LUMO, in add, the presence of heteroatom as nitrogen generate a no bond orbital between π and π^* orbitals.[48] Ligands **26** and **27** exhibit very similar values of maximum peaks.

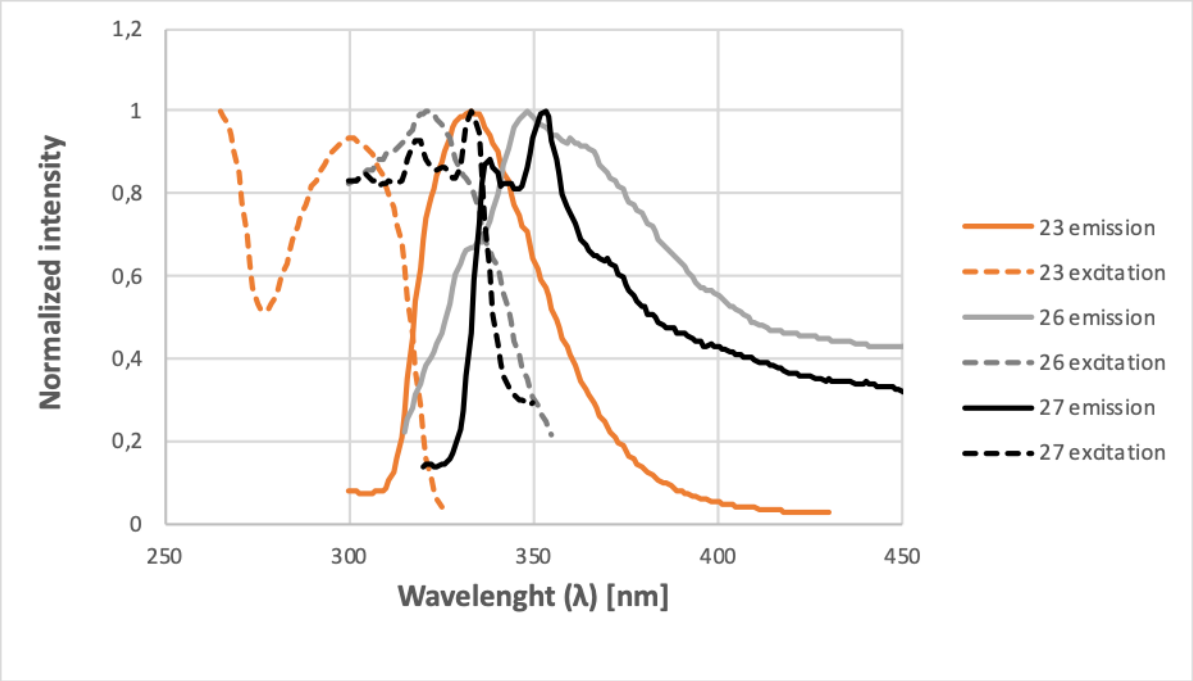

Figure 3.16: *Collected emission (full lines) and excitation (dashed lines) spectra of ligands (**23**, **26**, **27**). For emission spectra:* $\lambda_{excitation}$ (**23**) = 310 nm,*:* $\lambda_{excitation}$ (**26**, **27**) = 300 nm. For excitation spectra**:** $\lambda_{emission}$ (**23**) = 350 nm, $\lambda_{emission}$ (**26**, **27**) = 370 nm

Ligands **23**, **26**, **27** exhibit high emission intensity, high simmetry between excitation and emission spectra and low Stoke shift (the gap, expressed in wavenumbers, between the maximum of the first absorption band and the maximum of emission band), so the emission process can be described as fluorsence process, where the electron return to a singlet ground state (S_0) from a singlet excited state (S_1). Compared with their relative chelating ligands, complexes **44**, **45**, **47**, **48**, **49** have a lower intensity emission, lower simmetry between and higher gap between emission maxium and excitation maximum (figure 3.17)

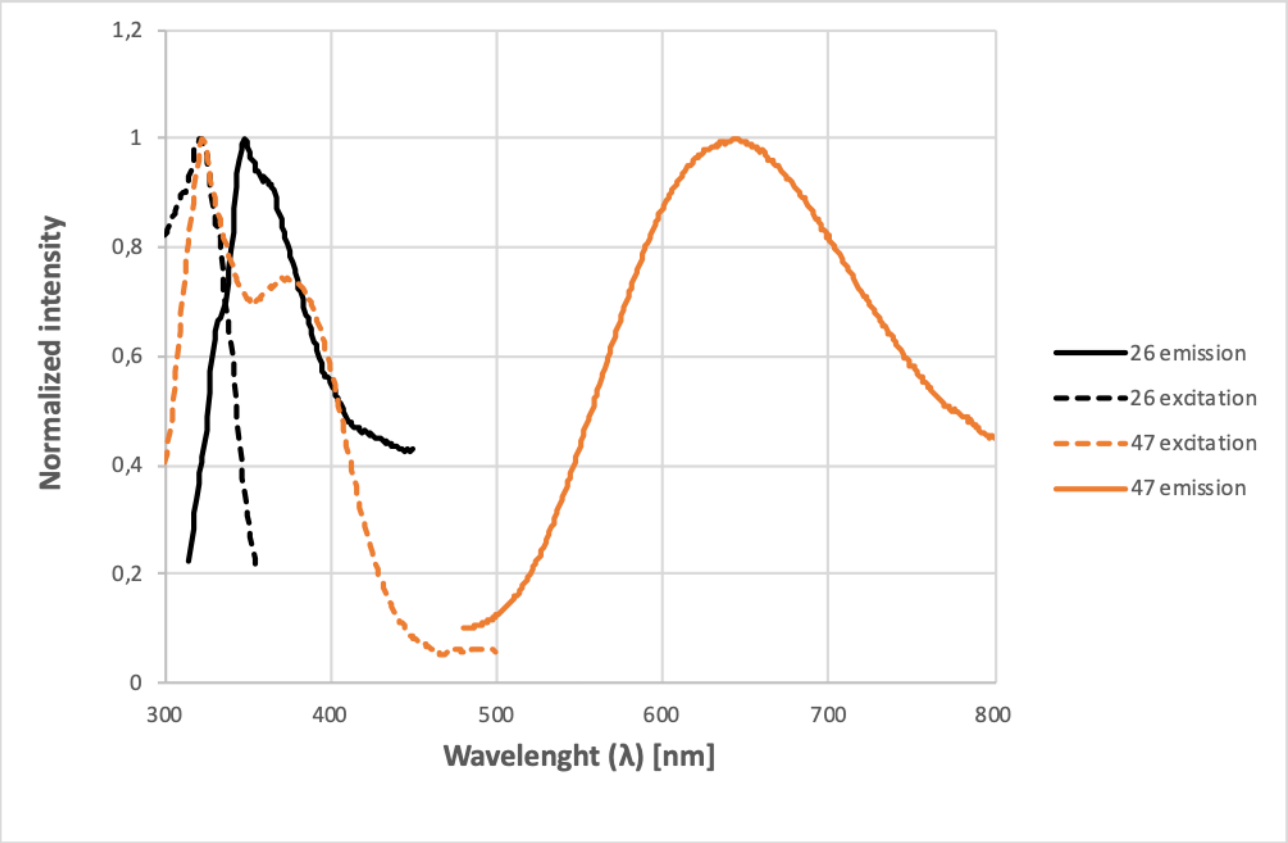

Figure 3.17: *Emission (full lines) and excitation (dashed lines) spectra for (**26**, **47**). For emission spectra:* $\lambda_{excitation}$ (**26**) = 300 nm, $\lambda_{excitation}$ (**47**) = 410 nm . For excitation spectra**:** $\lambda_{emission}$ (**26**) = 370 nm, $\lambda_{emission}$ (**47**) = 580 nm

These differences are attributable to a different kind of emission. In fact, these features are typical for phosporescence emissions. It is possible that electron from singlet excited state (S_1) pass to a triplet excite state (T_1) by ISC process. Then it can return to S_0 from T_1 by another ISC, this step can be accompained by light emission. The emitted radiation from phosporescence has a longer wavelenght than emitted radiation from fluorescence, because T_1 state has little lower energy than S_1. (All significant data are collected in Table 3.2)

Emission				Excitation		
Ligand	**λ_{max} [nm]**	**λ^{R}_{max} [nm]**	**λ_{sh} [nm]**	**λ_{max} [nm]**	**λ^{R}_{max} [nm]**	**λ_{sh} [nm]**
23	333	/	/	265	300	/
26	348	365	335	321	/	331
27	353	338	370	333	325 319	
44	399	/	/			
45	412	/	397	353	/	/
47	642	/	/	323	374	/
48	641	/	/	336	382	/
49	628	/	/	302	/	346

Table 3.2: *Emission and excitation data for ligands and complexes. λ^{R}_{max} is a relative maximum peak and λ_{sh} is a shoulder of a peak*

To confirm that complexes emission comes from a triple state, an additional analysis was performed. Oxygen ground state is triplet state and it is a very good triplet state quencher. It can quench molecules that stay in a triplet state to singlet state.

All complexes have been measured in Argon atmosphere, then, the inert atmosphere have been removed opening cuvette and the solutions have been shaken (for three times). The measurements of emission spectra have been repeated in oxygen atmosphere under the same conditions. The ratio between emission in the two different atmospheres are included from 0,3 to 0,56 so emission of these complexes involves a triple state (Table 3.3 and Figure 3.18).

Complex	**$\lambda_{emission}$ [nm]**	$\frac{Intensity\ emission\ in\ O_2\ atmosphere}{Intensity\ emission\ in\ Ar\ atmosphere}$
45	412	0,556
47	642	0,555
48	641	0,303
49	628	0,492

Table 3.3: *Intensity emission ratio in O_2 atmosphere and Ar atmosphere*

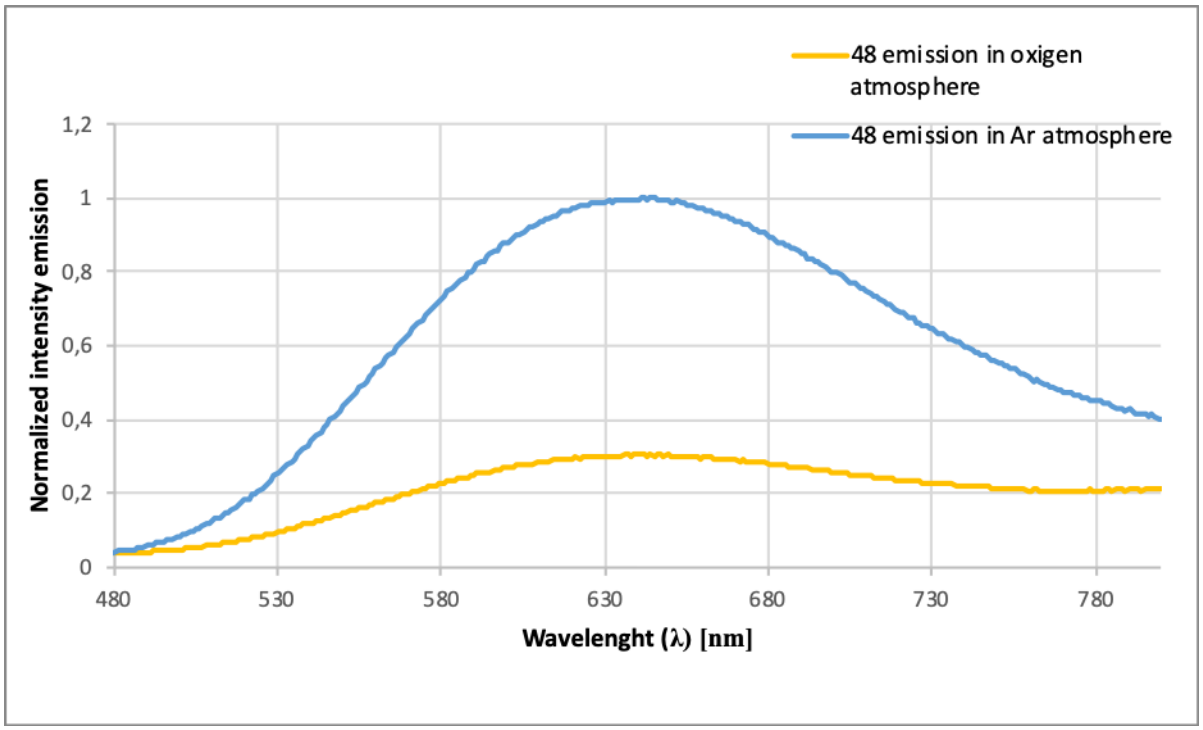

Figure 3.18: *Compared spectra of* ***48*** *in* O_2 *(orange line) and Ar (blu line) atmosphere.* $\lambda_{excitation}$ (**48**) = 410 nm

3.5 Electrochemical data

The electrochemical features of ligands and complexes are studied using cyclic voltammetry. All analysis were performed using dry CH_3CN as solvent and tetrabutylammoniumhexafluorophosphate ($TBAPF_6$) 0,1 M as supporting electrolyte. $TBAPF_6$ was crystalized twice in hot EtOH to increase purity. Supporting electrolyte has two important roles: it reduces the solution resistance and avoids analyte migration out of the measuring surface; solvent and support electrolyte must be electrochemical and chemical inert in the experimental condition. Experiments are conducted in a cylindrical cell with a three electrodes system: working electrode (WE), auxiliary electrode (AuxE) and a pseudo reference electrode (qRE). Pt disk is used as WE, Pt wire is used as AuxE and Ag wire is used as qRE. Unfortunately, the potential of Ag can change between experiments in different conditions (for example: different electrolyte or solvent), to solve this problem ferrocene (Fc) is added as internal standard. Ferrocene/ferrocenium couple (Fc/Fc^+) have a solvent-independent potential[49] and, using it is possible produce comparable outcomes. Fc is added with a concentration of 5 mM and analytes with a concentration between 5 mM and 10 mM, the analysis was conducted in O_2-free solutions. Unfortunately, during blank scan it is often observed two impurities peaks between -1,5 V and 0 V (vs Fc/Fc^+) and it was not possible removed them. All compounds are studied at four different scan rates: 50, 100, 200, 500 mV/s. Scan rate can influence several data. First of all: intensity current. In fact, increasing scan rata the gradient concentration between the

surface of electrode and the bulk of solution (δC/δx) increase and current intensity is linear dependent by δC/δx (until limit current). Another consequence of increasing scan rate is to shift the maximum intensity potential toward higher value, for cathode (E_c), and lower, for anode (E_a). The reversible grade is also influenced by scan rate (SR). Some reactions are reversible at low SR, but they became irreversible at higher SR. This phenomenon takes place because the reaction rate (RR) is dependent by SR. At low SR the reaction rate are lower then transfer matter rate at high SR is the opposite.[50],[51]

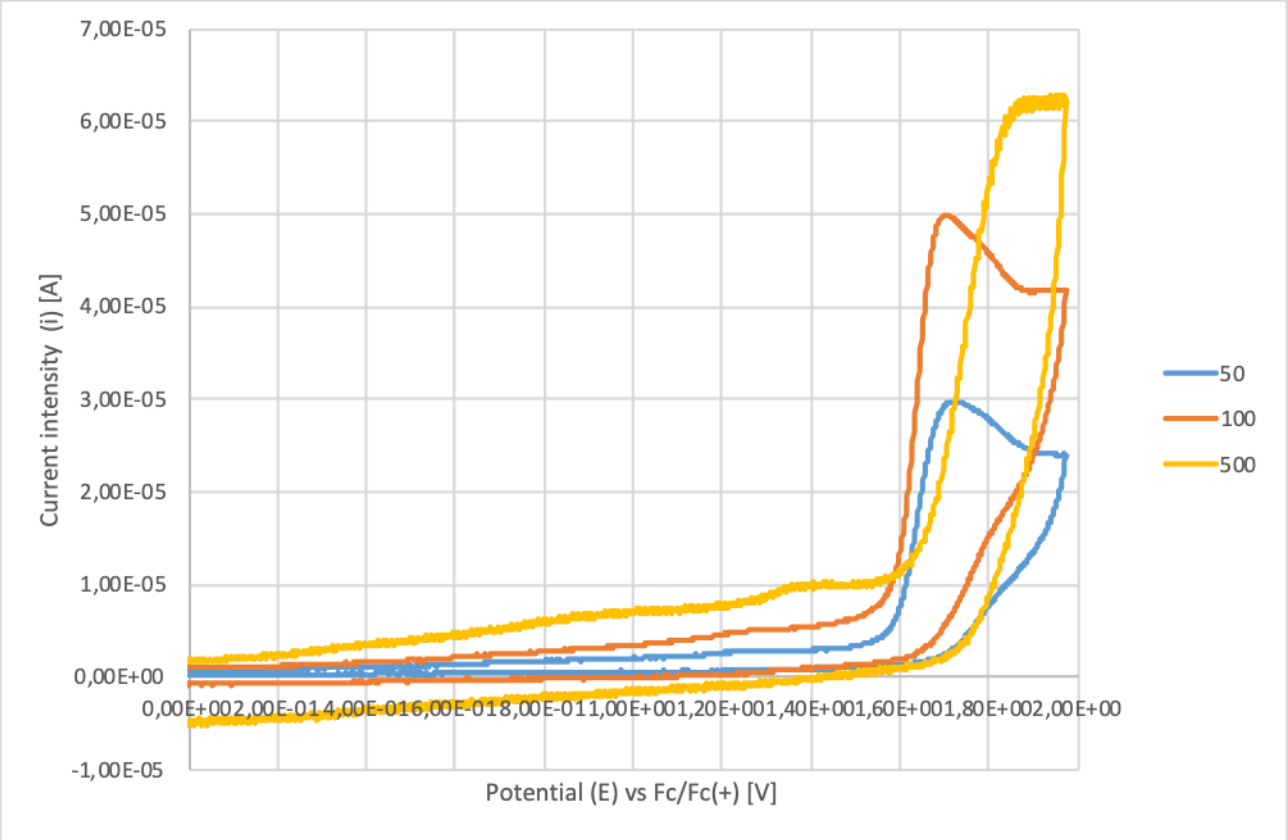

Figure 3.18: *Cyclic voltammetry for* ***24*** *at (50, 100, 500 mV/s)*

Complexes **44** and **45** exhibit a reversible peak, respectively, at -0,318 V and -0,613 V (vs Fc/Fc^+), these peaks are attributable to free $P(Ph_3)_3$.[52] $P(Ph_3)_3$ can be substituted by solvents with Lewis basis properties as ligand in Cu complexes. [37]

All compounds have shown irreversible processes. Ligands exhibit oxidation processes between 1,4 V and 1,7 V (vs Fc/Fc^+) and reduction processes between -2,0 V and -2,6 V (vs Fc/Fc^+). Unfortunately, in the electrochemical window used, it was not possible to observe all the potentials forseveral ligands. It might be possible to detect these signals using different solvent/supporting analyte solutions with a different electrochemical window. Complexes show oxidation processes

between 0,95 V and 1,45 V (vs Fc/Fc^+), complexes **47**, **48**, **49** exhibit two peaks. The first peaks is attributable to copper oxidation, the second peaks should concern a POP oxidation. In reduction, all signals are included from -2,8 V to -2,0 V (vs Fc/Fc^+), these processes are attributable to ligand reduction. [45]

	E ox [V]	**E red [V]**	**HOMO (eV)**	**LUMO (eV)**	**Δ HOMO-LUMO (eV)**
23	1,64	Not detected	-6,44	/	/
24	1,38	-2,08; -2,33	-6,18	-2,72	3,46
26	1,55	Not detected	-6,35	/	/
27	Not visible	-2,52	/	-2,28	/
44	1,35	-2,06; -2,33	-6,15	-2,74	3,41
45	1,30	Not detected	-6,10	/	/
47	1,35; 1,21	-2,80	-6,01	-2,00	4,00
48	1,28; 0,95 *	-2,40	-5,75	-2,40	3,35
49	1,43; 1,24	-2,43	-6,04	-2,37	3,67

Table 3.4: *Electrochemical properties for ligands (**23**, **24**, **26**, **27**) and complexes (**44**, **45**, **47**,**48**, **49**) at 100 mV/s * For complex **48**, the oxidation potentials are referred at 200 mV/s*

HOMO and LUMO levels are in relation with oxidation and reduction potential. Fc/Fc^+ potential is equal at 4,8 eV *versus* zero vacuum level, HOMO and LUMO values are estimated by adding the oxidation and reduction potential.[53]

Unfortunately, it was possible calculated HOMO-LUMO gap only for complexes **47**, **48**, **49.** No significant differences have been found with literature data. [45,46] HOMO-LUMO gap for complex **47** is suspicious, because it is higher than **49** HOMO-LUMO gap. It should be lower because, it exhibits higher absorption wavelength. All the electrochemical properties are reported in Table 3.4.

4 CONCLUSION

In this work five different heteroleptic Cu(I) complexes have been synthesized. Complexes **44** and **45** are mono-nuclear complexes composed by triimine ligand and $P(Ph_3)_3$, complexes **47** and **48** are tri-cationic complexes composed by bi-diimine mono-triimine ligand and POP and **49** is a di-nuclear complex composed by bi-diimine ligand and POP.

To take into consideration the employment of these complexes as photosensitizers, the following properties have been studied: redox potentials evaluated by cyclic voltammetry and absorptivity coefficient, absorption and emission evaluated by UV-Visible spectrophotometry and spectrofluorimetry. The synthesized complexes have shown good emission features and concordant outcomes with previous study. [45],[46] It was confirmed that quinoline instead of pyridine increase the π-conjugation of diimine ligand with the red shift of absorption in visible region.

The collected data are encouraging but they are not enough. To confirm the employment of these products as PS, different analysis should be done in future as excited time life, quantic yield and bimolecular quenching study.

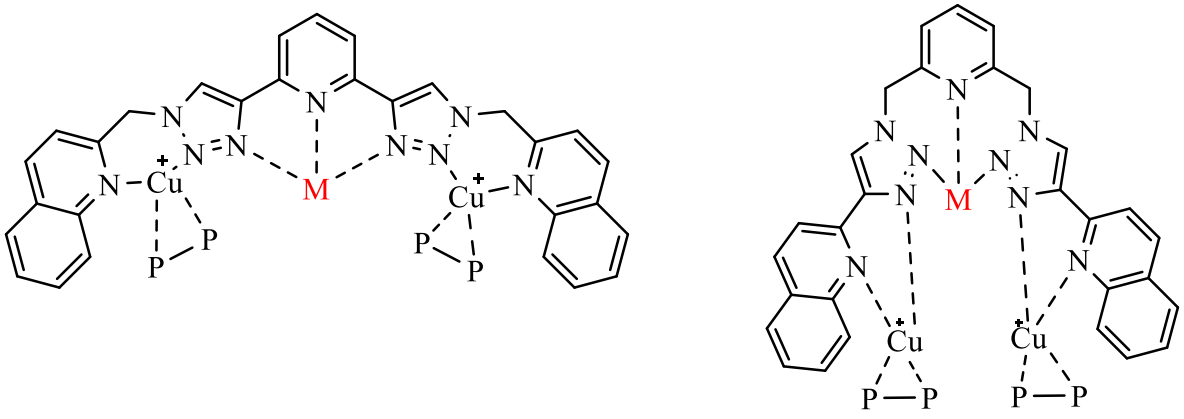

50 **51**

Figure 4.1: Hypothetical heteronuclear complexes (**50**, **51**) (M = metallic ion).

Ligands **26** and **27** have interesting structures, in fact they possess two different coordination sites. So, it should be possible produces heteronuclear complexes (**50**, **51**) where a coordination site host Cu^+ heteroleptic complexes with a photosensitizer function and in the other coordination site are situated another metallic ion (as Fe^0, Ni^{2+}, Co^{3+}). The aim of these product is the synthesis of a complex, which have PS and catalyst functionalities linked together.

5 Experimental section

5.1 Analytical Resources and Apparatus

The synthesized compounds were characterized by nuclear magnetic resonance (NMR). The NMR spectra were recorded using Bruker Avance 300 NMR, Bruker Avance 400 NMR and Bruker Avance 500 NMR. The NMR spectra were recorded at room temperature in deuterated solvents. The chemical shift δ is displayed in parts per million [ppm] and the references used were the ^{1}H and ^{13}C peaks of the solvents themselves: d1-chloroform ($CDCl_3$): 7.26 ppm for ^{1}H and 77.0 ppm for ^{13}C, methylene chloride ($CDCl_2$): 5.32 ppm for ^{1}H and 54.00 ppm for ^{13}C and d3-acetonitrile (CD_3CN):1.93 ppm for ^{1}H and 1.3 ppm for ^{13}C. When describing couplings, the following abbreviations were used: d = doublet, t = triplet, m = multiplet, dd = doublet of doublet, ddd = doublet of doublet of doublet. Coupling constants "*J*" are given in Hertz [Hz] with the largest value first.

The absorption spectra were recorded with a PerkinElmer Lambda 750 UV/Vis spectrometer. The measurements were performed at 20 °C. A correction of spectra was made automatically by the instrument with the absorption of the pure solvent (blank).

Luminescence properties were measured at room temperature using a Horiba-Fluoromax 13456 with integration time of 0.8 s.

5.2 Synthesis of ligands and complexes

5.2.1 Synthesis of 2-bromomethylquinoline [54]

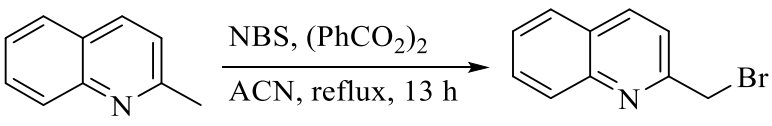

26 **27**

2-methylquinoline (95 mg, 0.664 mmol, 1 eq.), NBS (124 mg, 0.697 mmol, 1.05 eq), $(PhCO_2)_2$ (7 mg, 0.0266 mmol, 0.04 eq.), ACN (10 mL) were stirred at reflux for 4 h at reflux, afterwards NBS (50 mg), $(PhCO_2)_2$ (4 mg), ACN (2 mL) were added and the reaction was stirred at reflux for other 9 h. Then, the solvent was removed by rotatory evaporation, the crude was dissolved in dicloromethane (DCM) and the organic phase was washed with H_2O (x 3), brine (x 1) and dried over anhydrous Na_2SO_4. The product was purified by silica gel chromatographic column (CC)

(ethyl acetate/cyclohexane from 1:20 to 1:10). The product was a white crystal, but it could became dark purple after 2 days (72 mg, 0.332 mmol Y= 49%).

^{1}H-NMR (300 MHz, $CDCl_3$) δ 8,08 (m, 2H), 7,72 (dd, 1H), 7,67 (m, 1H), 7,48 (m, 1H), 7,47 (s, 2H).

5.2.2 Synthesis of 2,6-bis((trimethylsilyl)ethynyl)pyridine [55]

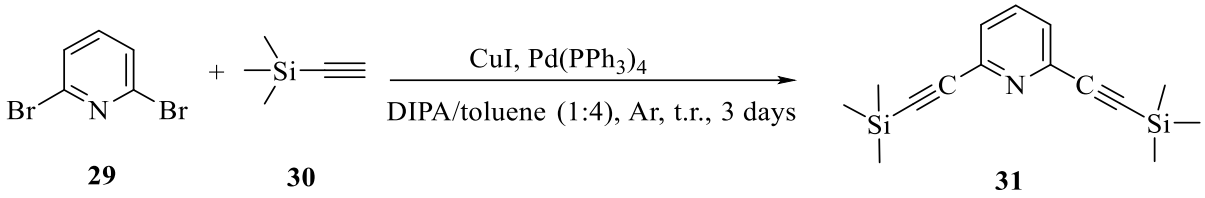

29 **30** **31**

The glassware was dried under Argon flow and heat. $Pd(PPh_3)_4$ (731.7 mg, 0.20 mmol, 0.2 eq.) and CuI (120.6 mg, 0.63 mmol, 0.3 eq.) were added to a solution of 2,6-dibromopyridine (500 mg, 2.11 mmol) in dry DIPA (3 mL) and dry toluene (13 mL) under Ar, then trimethylsilylacetilene (2.4 mL, 12.9 mmol, 8 eq) was added. The resulting mixture was stirred for 3 days at room temperature in Ar atmosphere. The solvent was removed by rotatory evaporation. The crude was purified by CC (cyclohexane/ethyl acetate 20:1). The product was a white crystal, it could degrade in air) (295 mg, 1,09 mmol, Y = 52 %).

^{1}H-NMR (300 MHz, $CDCl_3$) δ: 7,59 (m, 1H), dd (7,38, 2H), 0,26 (s, 18H)

5.2.3 Synthesis of 2,6-biethynylpyridine

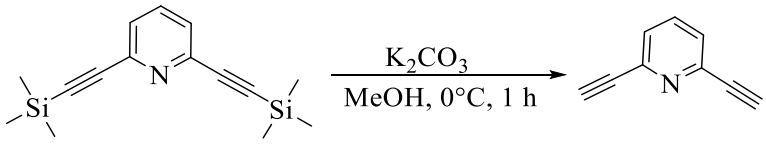

31 **32**

The product **31** (240 mg, 0.884 mmol) was dissolved in MeOH (15 mL), then the mixture reaction was cooled down at 0°C for 30 minutes in ice bath. Afterwards K_2CO_3 (367 mg, 2.65 mmol, 3 eq.) and the resulting mixtures was stirred for 1 h at 0°C. The solvent was removed by rotatory evaporation. The crude was dissolved in DCM and the organic phase was washed with H_2O (x 3)

and brine solution (x 1). The product was a yellow solid, but it was very instable and the yield was not calculated, so it was used quickly and completely in the next reaction.

^{1}H-NMR (300 MHz, $CDCl_3$) δ: 7,65 (m, 1H), dd (7,46, 2H), 3,15 (s, 1H)

5.2.4 Synthesis of 2,6-bis(1'-benzyl-1',2',3'-triazol-4'-yl)pyridine [56]

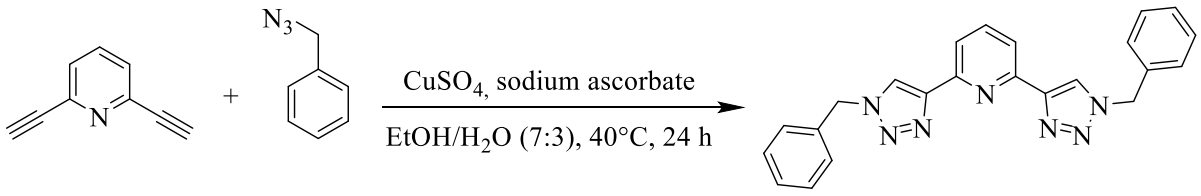

32 **33** **23**

To a stirred solution of **32** (112 mg, 0.884 mmol) in EtOH /H_2O 7:3 was added benzyl azide (0.331 µL, 1.768 mmol 2 eq.), $CuSO_4 \cdot 5\ H_2O$ (120 mg, 0.442 mmol, 0.5 eq.), sodium ascorbate (87.6 mg, 0.442 mmol 0.5 eq). The resulting solution was stirred at 40°C for 21 h. After 21 h benzyl azide (70 µL), $CuSO_4 \cdot 5\ H_2O$ (26 mg), sodium ascorbate (20 mg) were added. The resulting solution was stirred at 40°C for 3 h more. The solvent was removed by rotatory evaporation, the crude was dissolved in DCM and the organic phase was washed with NH_4OH in 25 %) (x 3), brine (x 1) and then it was dried over by Na_2SO_4. The product was crystallized in a solution of DCM/cyclohexane. The product was a white solid. (289 mg, 0,734 mmol, Y=83%)

^{1}H-NMR (300 MHz, CD_2Cl_2) δ 8.10 (s, 2H), 8.07 (s, 2H), 7.90 – 7.82 (m, 1H), 7.41 – 7.25 (m, 10H), 5.56 (s, 4H).

^{13}C-NMR (300 MHz, CD_2Cl_2) δ 150,953 (C), 149,408 (C), 138,487 (CH), 135,780 (C), 129,485 (CH), 129,450 (CH), 128,834 (CH), 122,935 (CH), 119,798 (CH), 55,035 (CH_2).

5.2.5 Synthesis of 2,6-bis(1'(2'-methylquinolinyl)-l',2',3'-triazol-4'-yl)pyridine

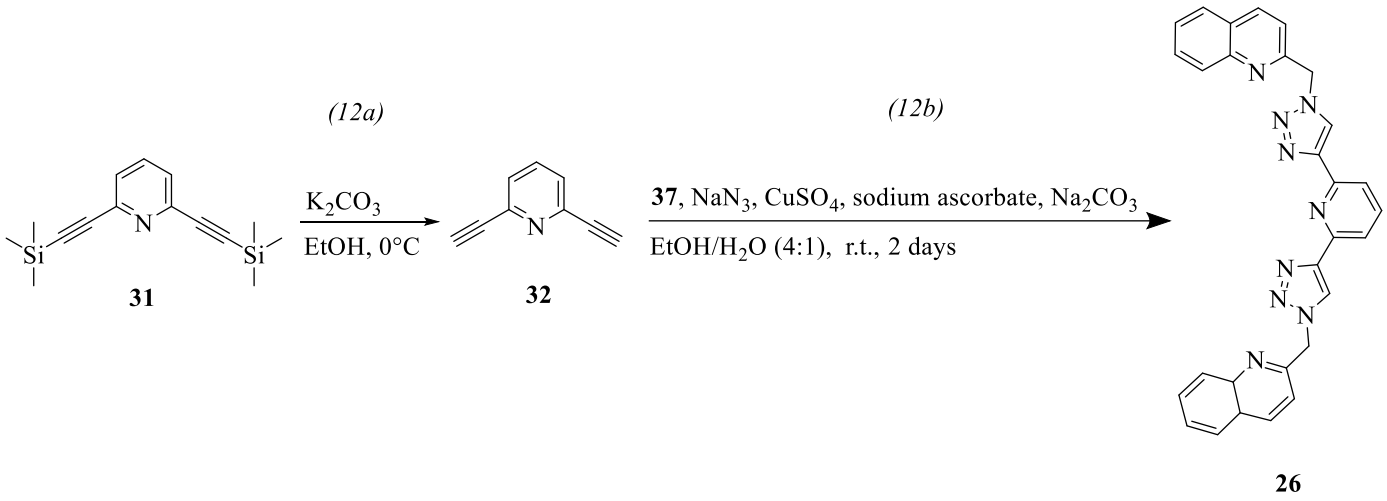

The product **31** (197 mg, 0.727 mmol) was dissolved in EtOH (15 mL), then the mixture reaction was cooled down at 0°C for 30 minutes in ice bath. Afterwards K_2CO_3 (502 mg, 4.42 mmol, 5 eq.) the resulting mixtures was stirred for 2 h at 0°C. Then, the ice bath was removed and, in stirred conditions, bromoquinaldine (323 mg, 1.454mmol 2 eq.), NaN_3 (189 mg, 2.908 mmol, 4 eq.), $CuSO_4 \cdot 5\ H_2O$ (181 mg, 0,727mmol, 1 eq.), sodium ascorbate (144mg, 0.727 mmol 1 eq.), Na_2CO_3 (85 mg, 0.727 mmol, 1 eq) was added. The resulting solution was stirred at room temperature for 30 h. After 30 h $CuSO_4 \cdot H_2O$ (62 mg), sodium ascorbate (40 mg), NaN_3 (50 mg) was added. The resulting solution was stirred at room temperature for other 18 h. The solvent was removed by rotatory evaporation the crude was dissolved in DCM and the organic phase was washed with NH_4OH (25%) (x 3), brine (x 1); the aqueous phases were collected and extracted with DCM, in the end all organic phases were dried over Na_2SO_4. The product was recrystallized from a solution of DCM/cyclohexane. The product was a white solid. (241 mg, 0,487 mmol, Y=67%)

^{1}H-NMR (300 MHz, CD_2Cl_2) δ 8.31 (s, 2H), 8.15 (d, J = 8.5 Hz, 2H), 8.03 (t, J = 9.0 Hz, 4H), 7.88 – 7.77 (m, 3H), 7.72 (ddd, J = 8.5, 6.9, 1.7 Hz, 2H), 7.56 (ddd, J = 8.3, 6.9, 1.4 Hz, 2H), 7.31 (s, 2H), 5.85 (s, 4H).

^{13}C-NMR (300 MHz, CD_2Cl_2): 155,445 (C), 150,998 (C), 149,438 (C), 148,554 (C), 138,453 (CH), 138,354 (CH), 130,833 (CH), 129,961 (CH), 128,505 (CH), 127,808 (CH), 123,817 (CH), 120,363 (CH), 119,781 (CH), 100, 827 (C), 57,192 (CH_2)

5.2.6 Synthesis of 2,6-bis((4'-phenyl-1',2',3'-triazol-1'-yl)methyl)pyridine

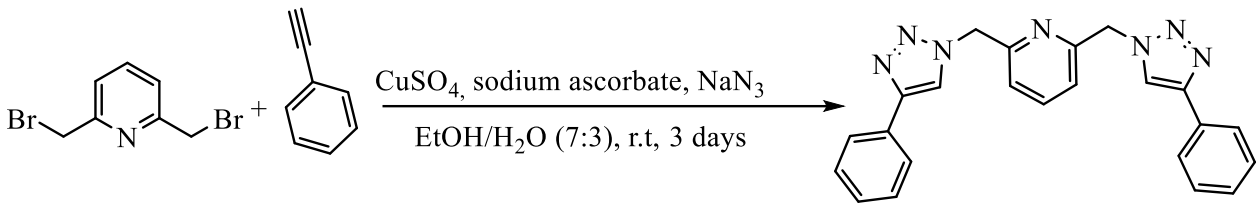

34 **35** **24**

To a stirred solution of 2,6- bis(bromomethyl)pyrdine (662 mg, 2.5 mmol) in EtOH /H_2O 7:3 (20 mL) was added NaN_3 (650 mg, 10 mmol 4 eq.), $CuSO_4 \cdot 5\ H_2O$ (624 mg, 2.5 mmol, 1 eq), sodium ascorbate (495 mg, 1 mmol, 1 eq), Na_2CO_3 (249 mg, 3.0 mmol, 1,2 eq), ethynylbenzene (548 µL, 5 mmol, 2 eq.). The resulting solution was stirred at room temperature for 3 days. The solvent was removed by rotatory evaporation, the product was washed in DCM, cyclohexane, ethyl acetate, it was not soluble in these solvents, so it was filtered by Buchner's filtering funnel. The product was a white crystal.(0,588 g, 1,495 mmmol, Y=60%.)

^{1}H-NMR (300 MHz, CD_2Cl_2) δ 7.92 (s, 2H), 7.83 – 7.68 (m, 5H), 7.45 – 7.26 (m, 6H), 7.22 (d, J = 7.7 Hz, 2H), 5.68 (s, 4H).
^{13}C-NMR (300 MHz, CD_2Cl_2) δ 155,109 (C), 148,667 (C), 139,558 (CH), 131,482 (C), 129,633 (CH), 128,896(CH) 126,361 (CH), 122,687 (CH), 121,275 (CH), 56,097 (CH_2)

5.2.7 Synthesis of 2-(trimethylsilylethynyl)quinoline

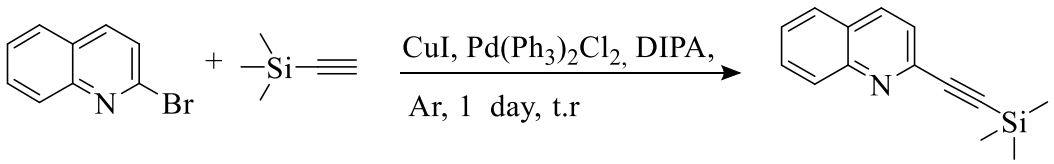

28 **20** **29**

The reaction enviroment was dried by Argon flow and warm. $PdCl_2(PPh_3)_2$ (84 mg, 0.12 mmol, 0.05 eq.) and CuI (69mg, 0.63 mmol, 0.15 eq.) were added to a solution of 2-bromoquinoline (500 mg, 2,4 mmol) in dry DIPA (25 mL) under Ar, then trimethylsilylacetilene (1.66 mL, 12 mmol, 5 eq) was added. The resulting mixture was stirred for 1 day at room temperature in Ar atmosphere. The solvent was removed by rotatory evaporation. The product was purified by silica gel CC

(cyclohexane/ethyl acetate from 25:1 to 10:1). The product was a white crystal (85,3 mg, 0,379 mmol, Y = 16%).

^{1}H-NMR (300 MHz, $CDCl_3$): δ 8.11 (1H, d), 8.08 (1H, d,), 7.77 (1H, d,), 7.69 (1H, dd,), 7.54 (1H, dd,), 7.52 (1H, d), 0.29 9H, s,).

*5.2.*8 Synthesis of 2,6-bis((4'-quinolin-2'-yl-1',2',3'-triazol-1'-yl)methyl)pyridine

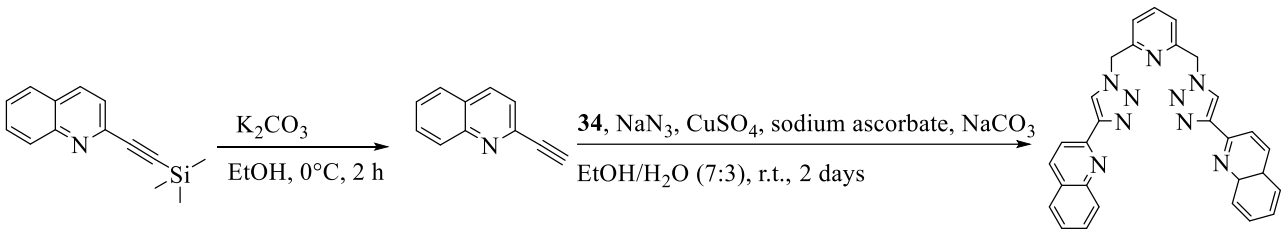

39 **40** **27**

The product **39** (78.2 mg, 0.347 mmol, 1 eq) was dissolved in EtOH (21 mL), then the mixture reaction was cooled down at 0°C for 30 minutes in ice bath. Afterwards K_2CO_3 (144 mg, 1.04 mmol, 3 eq) the resulting mixtures was stirred for 2 h at 0°C. Then, the ice bath was removed and in stirred conditions 2,6-dibromomethylpyridine (46 mg, 0.173 mmol, 0.5 eq.), NaN_3 (45 mg, 0.694 mmol, 2 eq), $CuSO_4{\cdot}5H_2O$ (43 mg, 0.173 mmol, 0.5 eq.), sodium ascorbate (35 mg, 0.173 mmol 0.5 eq), Na_2CO_3 (18 mg, 0.173 mmol, 0.5 eq) were added. The resulting solution was stirred at room temperature for 2 days. The solvent was removed by rotatory evaporation, the crude was dissolved in DCM and the organic phase was washed with NH_4OH (25%) (x 3), brine (x 1); the aqueous phases were collected and extracted with DCM, the collected organic phases were dried over Na_2SO_4. The product was crystallized in a solution of DCM/cyclohexane. The product was a green solid (29 mg, 0.0586 mmol Y=34%).

^{1}H-NMR (500 MHz, $CDCl_3$) δ 8.50 (s, 2H), 8.30 (d, J = 8.5 Hz, 2H), 8.18 (d, J = 8.6 Hz, 2H), 8.01 (d, J = 8.5 Hz, 2H), 7.80 (dd, J = 8.1, 1.5 Hz, 2H), 7.72 – 7.64 (m, 3H), 7.51 (ddd, J = 8.0, 6.8, 1.2 Hz, 2H), 7.24 (d, J = 7.8 Hz, 2H), 5.78 (s, 4H).

^{13}C-NMR (500 MHz, $CDCl_3$) δ 153,713 (C), 150,406 (C), 149,196 (C), 148, 088 (C), 138,918 (CH), 137,054 (CH), 129,888 (CH), 129,173 (CH), 127,931 (C), 127, 894 (CH), 126,539 (CH), 123,644 (CH), 122,230 (CH), 118,805 (CH), 55,703 (CH_2).

5.2.9 Synthesis of 1-(methylquinol-2'-yl)-4-phenyl-1,2,3-triazole

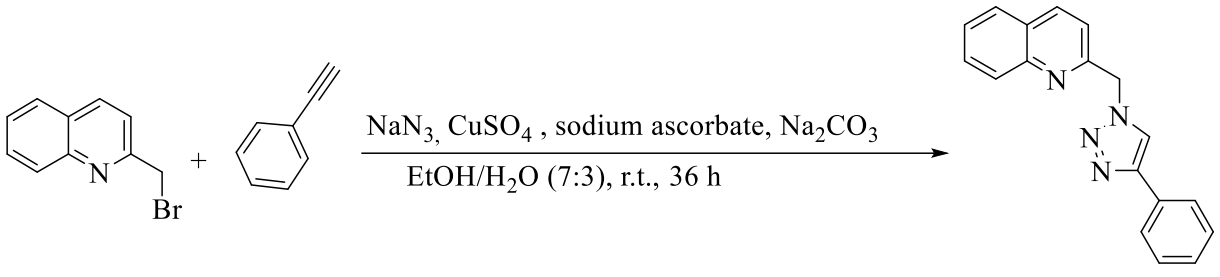

37 **35** **25**

To a stirred solution of 2-bromomethylquinoline (60 mg, 0.271 mmol 1 eq) in EtOH /H_2O 7:3 (10 mL) were added NaN_3 (35,2 mg, 0,542 mmol,2 eq.), $CuSO_4 \cdot H_2O$ (34 mg, 0.136 mmol, 0.5 eq.), sodium ascorbate (27 mg, 0.136 mmol, 0.5 eq), Na_2CO_3 (14 mg, 0.163 mmol, 0.6 eq), ethynylbenzene (30 μL, 0.271 mmol, 1 eq.). The resulting mixture was stirred at room temperature for 36 h. The solvent was removed by rotatory evaporation, the crude was dissolved in DCM and the organic phase was washed with NH_4OH 25 %) (x 3), brine (x 1) and then it was dried over by Na_2SO_4. The product was purified by a gel CC (from ethyl acetate/cyclohexane 1:10 to 100% ethyl acetate. The product was a white solid (49 mg, 0,171 mmol, Y=63%).

^{1}H-NMR (300 MHz, $CDCl_3$) δ 8.16 (dd, J = 8.5, 0.8 Hz, 1H), 8.09 (dd, J = 8.2, 0.9 Hz, 1H), 7.93 (d, J = 1.7 Hz, 1H), 7.85 – 7.78 (m, 3H), 7.78 – 7.72 (m, 1H), 7.58 (ddd, J = 8.2, 6.9, 1.3 Hz, 1H), 7.44 – 7.35 (m, 2H), 7.36 – 7.27 (m, 2H), 5.89 (s, 2H).

5.2.10 Synthesis of **44**

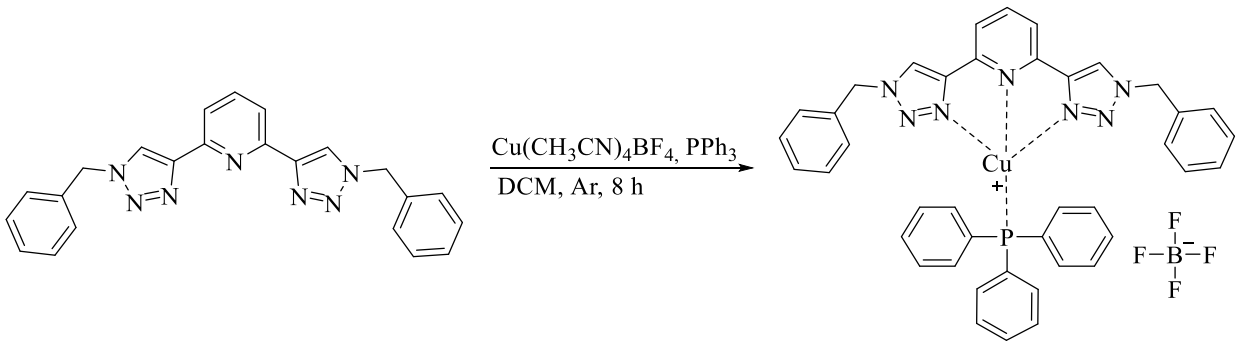

23 **44**

The reaction was conducted with a Schlenk technique. The glassware was dried by Ar flow and heat. $Cu(CH_3CN)_4BF_4$ (77 mg, 0.95 mmol, 0.95 eq) and PPh_3 (63 mg, 0.241 mmol, 0.95 eq) were

dissolved in dry DCM (6 mL), the mixture stirred for 30 minutes. Then, the product **23 (**100 mg, 0.254 mmol, 1 eq) in 3mL of dry DCM was added. After 8 h the solvent was removed by rotatory evaporation. The product was crystallized in a solution of DCM/ cyclohexane. The product is solid (167 mg, 0,208 mmol, Y=86%).

^{1}H-NMR (300 MHz, CD_2Cl_2) δ 7,38 (m, 10H), 7,20 (m, 13H), 6,94 (m, 7H), 5,29 (s, 4H)
^{13}C-NMR (300 MHz, CD_2Cl_2) δ 147,242 (C), 139,010 (CH), 134,120 (CH), 133,913 (CH), 133,551 (C), 133,112 (C), 130,784 (CH), 130,113 (CH), 130,012 (CH), 129,934 (CH), 129,389 (CH), 129,262 (CH), 124,184 (C), 55,875 (CH_2)

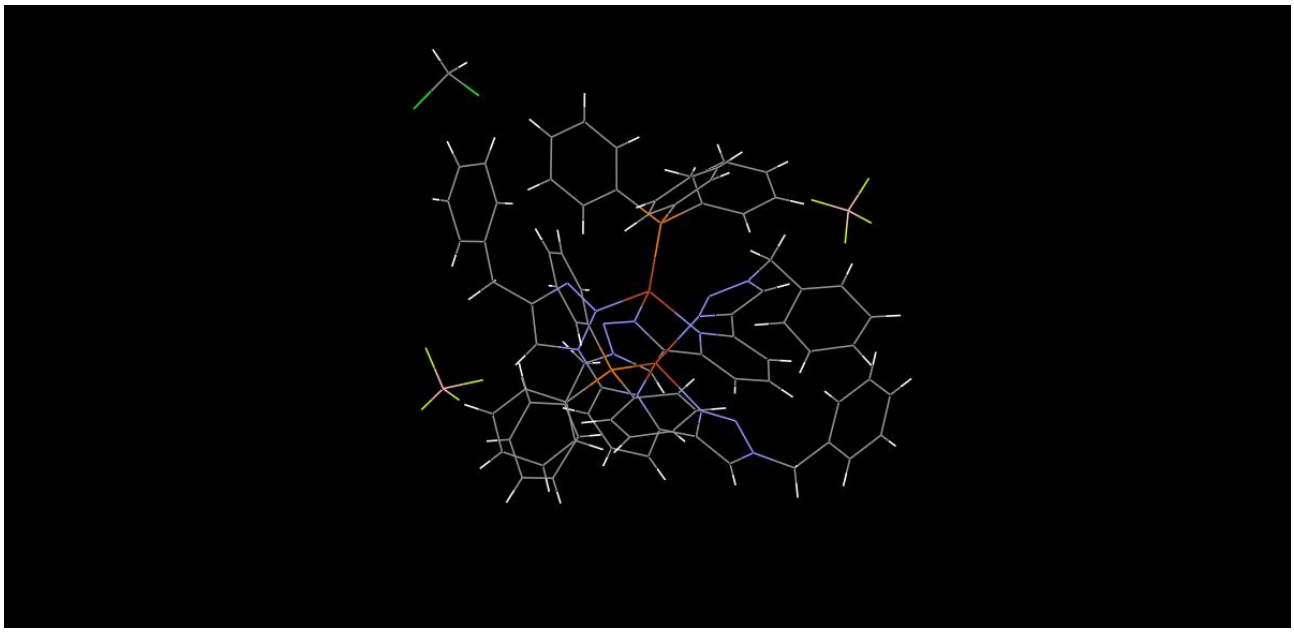

Figure 5.1 *X-ray structure for complex* ***44***

Atom	**Atom**	**Length/Å**		**Atom**	**Atom**	**Atom**	**Angle/°**
Cu1	P1	2.1999		N3	Cu1	P1	122.81
Cu1	N3	2.141		N4	Cu1	P1	119.56
Cu1	N4	2.109		N4	Cu1	N3	78.67
Cu1	N13	2.060					

Table 5.1 *Some relevant data for X-ray structure of complex* ***44***

5.2.11 Synthesis of **45**

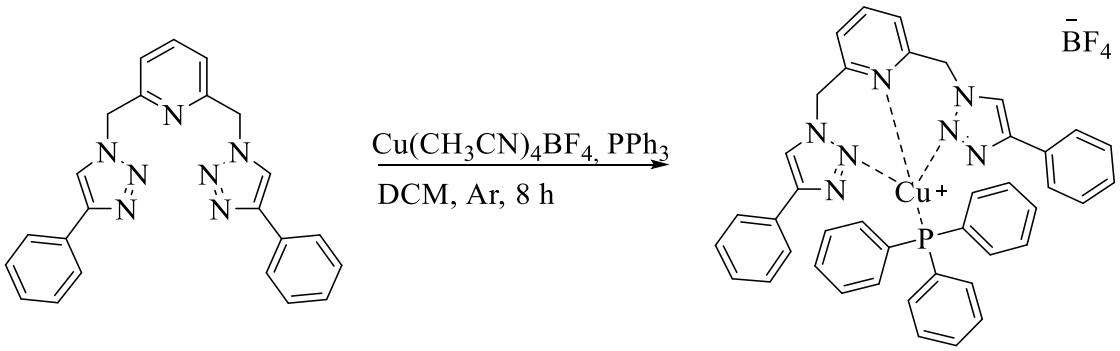

24 **45**

The reaction was conducted with a Schlenk technique. The glassware was dried by Ar flow and heat. $Cu(CH_3CN)_4BF_4$ (77 mg, 0.95 mmol, 0.95 eq) and PPh_3 (63 mg, 0.241 mmol, 0.95 eq) were dissolved in dry DCM (6 mL), the mixture stirred for 30 minutes. Then, the product **24 (**100 mg, 0.254 mmol, 1 eq) in 3mL of dry DCM was added. After 8 h the solvent was removed by rotatory evaporation. The product was crystallized in a solution of DCM/ cyclohexane. The product is solid (134 mg, 0,166 mmol, Y=69%).

^{1}H-NMR (300 MHz, CD_2Cl_2) δ 8,35 (s, 2H), 7,83(m, 7H), 7,38 (m, 21H), 5,53(s, 4H)
^{13}C-NMR (300 MHz, CD_2Cl_2) δ 152,757 (C), 149,146 (C), 141,507 (CH), 134,013 (CH), 133,815 (CH), 133,331 (C), 132,855 (C), 131,384 (CH), 130,002 (CH), 129,873 (CH), 129,692 (CH), 129,573 (CH) 129,657 (CH), 54,650 (C).

5.2.12 Synthesis of **47**

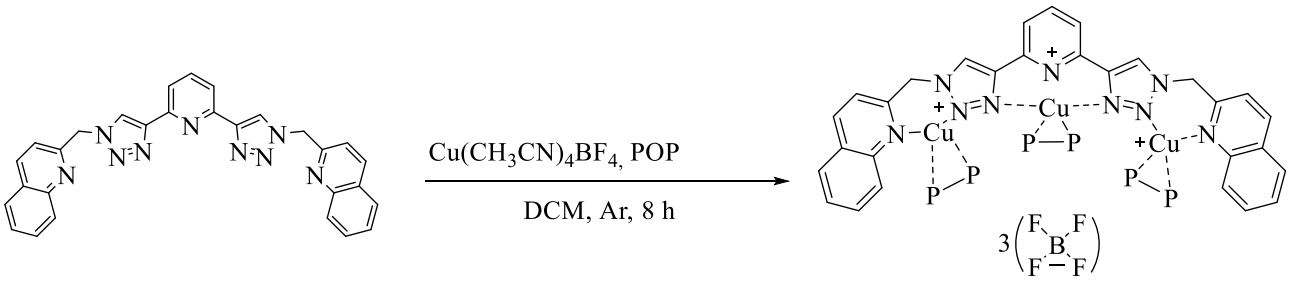

26 **47**

The reaction was conducted with a Schlenk technique. The glassware was dried by Ar flow and heat. $Cu(CH_3CN)_4BF_4$ (311 mg, 0.988 mmol, 3.28 eq) and POP (487 mg, 0.904 mmol, 3 eq) were dissolved in dry DCM (6 mL), the mixture stirred for 30 minutes. Then, the product **26 (**149 mg,

0.301 mmol, 1 eq) in 3mL of dry DCM was added. After 8 h the solvent was removed by rotatory evaporation. The product was crystallized in a solution of DCM/ cyclohexane. The product is solid (134 mg, 0,166 mmol, Y=91%)

1H NMR (300 MHz, CD3CN) δ 8.64 (s, 2H), 8.20 (d, J = 8.4 Hz, 2H), 7.91 (d, J = 8.0 Hz, 5H), 7.79 (d, J = 8.5 Hz, 3H), 7.69 (t, J = 7.5 Hz, 3H), 7.59 (t, J = 7.4 Hz, 3H), 7.40 – 7.11 (m, 83H), 6.89 (d, J = 7.1 Hz, 13H), 6.73 (d, J = 5.1 Hz, 6H), 5.57 (s, 4H).

5.2.13 Synthesis of **48**

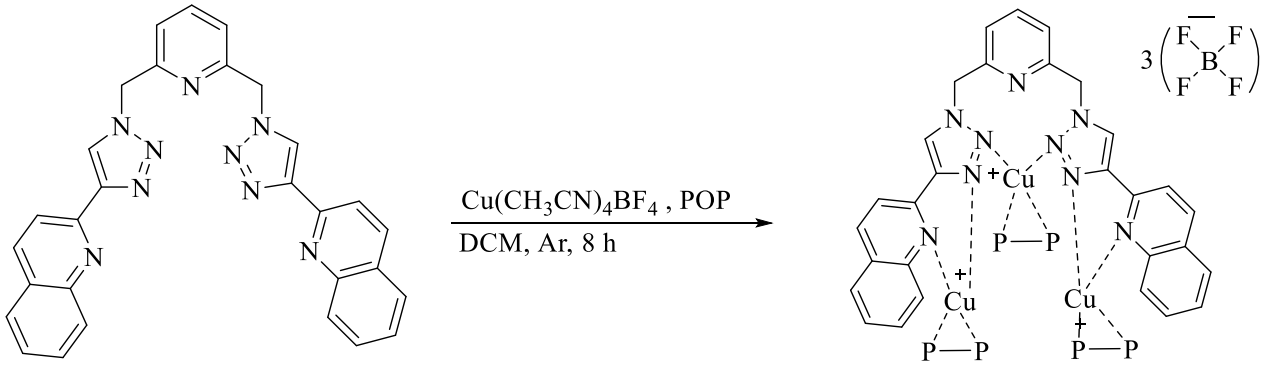

27 **48**

The reaction was conducted with a Schlenk technique. The glassware was dried by Ar flow and heat. $Cu(CH_3CN)_4BF_4$ (94 mg, 0.299 mmol, 5.10 eq) and POP (84 mg, 0.156 mmol, 2,66 eq) were dissolved in dry DCM (6 mL), the mixture stirred for 30 minutes. Then, the product **27 (**29 mg, 0.0586 mmol, 1 eq) in 3mL of dry DCM was added. After 8 h the solvent was removed by rotatory evaporation. The product was crystallized in a solution of DCM/ cyclohexane. The product is solid (52,7 mg, 0,0207 mmol, Y= 35%).

^{1}H-NMR (500 MHz, CD_2Cl_2) δ 8.99 (s, 2H), 8.47 (d, J = 8.5 Hz, 2H), 8.14 (d, J = 8.5 Hz, 2H), 7.94 (d, J = 8.6 Hz, 2H), 7.84 (d, J = 8.2 Hz, 2H), 7.65 (d, J = 7.8 Hz, 1H), 7.49 (d, J = 6.3 Hz, 8H), 7.46 – 7.20 (m, 36H), 7.10 (d, J = 8.0 Hz, 11H), 6.90 (m, 19H), 6.77 (s, 3H), 6.64 (m, 11H), 5.77 (s, 4H).

5.2.14 Synthesis of **49**

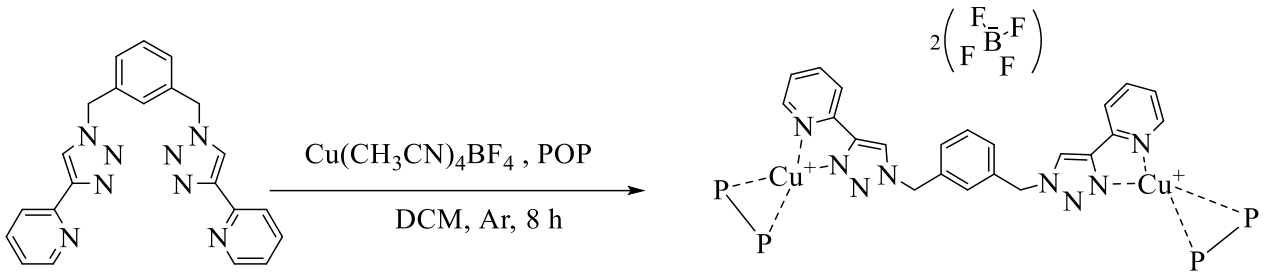

28 **49**

The reaction was conducted with a Schlenk technique. The glassware was dried by Ar flow and heat. $Cu(CH_3CN)_4BF_4$ (147 mg, 0.468 mmol, eq) and POP (252 mg, 0.468 mmol, 2,66 eq) were dissolved in dry DCM (6 mL), the mixture stirred for 30 minutes. Then, the product **28 (**98 mg, 0.248 mmol, 1 eq) in 3mL of dry DCM was added. After 8 h the solvent was removed by rotatory evaporation. The product was crystallized in a solution of DCM/ cyclohexane. The product is a yellow solid (445 mg, 0,248 mmol, Y=100%)

^{1}H-NMR (500 MHz, CD_2Cl_2) δ 8.81 (s, 2H), 8.00 – 7.95 (m, 4H), 7.88 (td, J = 7.8, 1.5 Hz, 2H), 7.75 (s, 1H), 7.45 – 7.36 (m, 8H), 7.33 (q, J = 5.3, 3.7 Hz, 5H), 7.30 – 7.22 (m, 14H), 7.20 (d, J = 1.4 Hz, 8H), 7.09 (ddd, J = 7.6, 5.2, 1.2 Hz, 3H), 7.06 – 6.92 (m, 17H), 6.78 – 6.69 (m, 12H), 5.58 (s, 4H)

^{13}C-NMR (500 MHz, CD_2Cl_2) δ 158,352 (C), 149,465 (CH), 147,362 (C), 146,234 (C), 138,983 (C), 135,572 (CH), 134,683 (CH), 132,614 (CH), 132,210 (CH), 130,730 (CH), 129,953 (CH), 128,875 (CH), 125,262 (CH), 124,859 (CH), 124,146 (CH), 122,402 (CH), 121,987 (CH), 55,032 (CH_2).

6 BIBLIOGRAPHY

[1] V. Smil, *Energy in Nature and Society: General Energetics of Complex Systems*, cap.XII, MIT Press, Cambridge, MA (USA), **2008**

[2] Department of Economic and Social Affairs, Population division, *World Mortality Report* 2005, United Nations Publication Sales No. E.06.XIII.3, **2006**

[3] M. Aresta, *Carbon Dioxide as Chemical Feedstock*, ed. M. Aresta, Wiley-VCH, Weinheim, **2010**, cap I, III,XIII

[4] N. Armaroli, V. Balzani, *Chem. Eur. J.*, **2016**, *22*, 32 – 57

[5] G. Ciamician, *Science*, **1912**, Vol. XXXVI. No 926

[6] N. Armaroli, V. Balzani, *Energy for a Sustainabke World – From the Oil Age to a Sun Powered Future*, Wiley-VCH, Weinheim (Germany), **2011**

[7] B. Wardle, *Principles and Applications of Photochemistry*, **2009**

[8] IEA (International Energy Agency), Renewable Energy Medium-Term Market Report, IEA technical report, **2014**

[9] G. Kavlak, J. McNerney, R. L. Jaffe, J. E. Trancik, *Energy Environ. Sci*. ,**2015**, 8, 1651–1659.

[10] Bach, U., Lupo, D., Comte, P. *et al.* Solid-state dye-sensitized mesoporous TiO_2 solar cells with high photon-to-electron conversion efficiencies. *Nature* 395**,** 583–585 (**1998**).

[11] K. A. Mazzio, C. K. Luscombe, *Chem. Soc. Rev.***, 2015**, 44, 78

[12] F. C. Krebs, N. Espinosa, M. Hosel, R. R. Sondergaard, M. Jorgensen, *Adv. Mater*. **2014**, 26, 29–39.

[13] D.L. Nelson, M.M.Cox, *Introduzione alla biochimica di Lehninger*, **2015**

[14] J. Barber, *Chem. Soc. Rev.*, **2009**, 38, 185–196

[15] Kumar et al., *Annu. Rev. Phys. Chem*. **2012.** 63, 541–69

[16] Amatore C, Sav´ean., *J. Am. Chem. Soc* **1981**. 103, 5021–23

[17] Hori Y, Wakebe H, Tsukamoto T, Koga O. *Electrochim. Acta*, **1994**, 39, 1833–39

[18] S. Berardi, et al, *Chem. Soc. Rev*., **2014,** 43, 7501-7519

[19] F. Liang Chan, G. Altinkaya, N. Fung, A. Tanksale, *Catalysis Today*, **2018**, 309, 242-247

[20] W.M. Sears,S. Roy Morrison, *J. Phys. Chem*. **1985**, 89, 3295-3298

[21] D.P. Summers, S. Leach, K.W. Frese Jr., *J Electroanal. Chem***., 1986**, 205, 219-232

[22] Gattrell , M. , Gupta , *J. Electroanal. Chem.*,**2006,** 594 , 1 – 19

[23] Kedzierzawski P, Augustynski J. *J. Electrochem. Soc.* **1994**, 141, 58–60

[24] J.M Lehn, R. Ziessel, *Proc. Natl. Acad. Sci*, **1982**, 79,701-704

[25] J. Agarwal, R. P. Johnson, G. Li, *J. Phys. Chem.*, **2011,** 2877-2881

[26] Sato S, Koike K, Inoue H, Ishitani O. *Photochem. Photobiol. Sci.* **2007**, 6. 454–61

[27] D. Nocera, D. Guldi, *Chem. Soc. Rev.*, **2009**, 38, 89–99

[28] Y. Pellegrin, F.Odobel, *C.R. Chemie*, **2017**, 20, 283-295

[29] Yui *et al.*, *Top Curr Chem*, **2011**, 303,151-184

[30] www.usgs.gov/centers/nmic/copper-statistics-and-information

[31] www.usgs.gov/centers/nmic/platinum-group-metals-statistics-and-information

[32] Armaroli *et. al*, *Top. Curr. Chem.*, **2007**, 280, 69-115

[33] D. R. McMillin, J. R. Kirchhoff, K.V Goodwin, *Coord. Chem. Rev.*, **1985**, 64, 83-92

[34] M.T. Miller, P. K. Gantzel, T. B. Karpishin, *Inorg. Chem.* **1998**, 37, 2285-2290

[35] D. R. McMillin *et al*, *J. Am. Chem. Soc.*, **2002**, 124, 6-7

[36] McCormick T, Jia WL, Wang SN, *Inorg. Chem.*, **2006**, 45, 147–155

[37] L. Bergmann, C. Braun, M. Niegerc , S. Bräse, *Dalton Trans*., **2018**, 47, 608

[38] Kuang, S.-M.; Cuttell, D. G.; McMillin, D. R.; Fanwick, P. E.; Walton, R. A. *Inorg. Chem.* **2002,** 41, 3313−3322.

[39] Y. Zhang *et al., Coord. Chem. Rev.* ,**2018**, 356, 127–146

[40] C. E. McCusker, F.N Castellano, *Inorg. Chem*. **2013**, 52, 8114−8120

[41] R. Huisgen *Proc. Chem. Soc.,* **1961,** 357-396

[42] (a) V. V. Rostovtsev, L. G. Green, V. V. Fokin, K. B. Sharpless, *Angew. Chem. Int. Ed.* **2002**, *41*, 2596; (b) F. Himo, T. Lovell, R. Hilgraf, V. V. Rostovtsev, L. Noodleman, K. B. Sharpless, V. V. Fokin, *J. Am. Chem. Soc.* **2005**, *127*, 210. (c) B. T. Worrell, J. A. Malik, V. V. Fokin, *Science* **2013**, *340*, 457.

[43] Stefan Bräse, C Gil, K. Knepper, V. Zimmermann, *Angew. Chem. Int.*, **2005**, 44, 5188 – 5240

[44] Clayden, Warren *et al*., *Organic Chemistry* 2nd Ed. – OUP **2012**

[45] C. Bizzarri *et al., Journal of Organometallic Chemistry*, **2018**, 871, 140-149

[46] L. Luci, Synthesis of heteroleptic Cu(I) complexes based on quinolin-yl-1*H*-1,2,3-triazole, **2018.** (Thesis has not been opened to public yet)

[47] T. Brandhofer *et al*, *Chem. Eur. J.* **2019**, 25, 4077 – 4086

[48] B. Valeur, *Molecular Fluorescence: Principles and Applications,* **2001**

[49] R. R. Gagne, C.A. Koval, G.C. Lisensky, *.Inorg. Chem*. **1980**, 19, 2855-2857

[50] G.A. Mabbott, *J. Chem. Educ.* **1983**, 60, 9, 697

[51] A. J. Bard, L.R. Faulker, *Electrochemical methods: Fundamentals and Applications,* **2001**

[52] *Electroanalytical Chemistry and Interracial Electrochemistry*, **1973**, 48, 425-431

[53] M. Thelakkat, H.W. Schmidt, *Adv. Mater*., **1998**, *10*, 219.

[54] Wen Zun Bi *et al*, *Tetrahedron*, **2018**, 74, 15, 1908 – 1917

[55] J. Carvalho *et* al, *J. Med. Chem*. **2013**, 56, 2828– 2840

[56] J. Kraft *et* al, Synthesis *(Germany)*, **2015**, 47, 199 – 208